Fig. 4. Invasion of immune or inflammatory cells into the graft. **A:** Immunohistochemistry of the graft at 24 hr, 72 hr, and 4 weeks with or without gfrMG is shown. Host-derived pan-leukocytic CD45-positive cells (red) invaded the region of the grafted cells (green) but never went beyond the border between the brain and gfrMG at 24 hr. **B:** The invasion was significantly reduced in the graft with gfrMG at 24 hr but increased with time until the difference became insignificant at 72 hr or 4 weeks (n = 3 in each group, $\star P < 0.05$). Scale bars = 200 μm.

Conventional MG includes growth factors such as FGF-2 (0–0.1 pg/ml), EGF (0.5–1.3 ng/ml), IGF-1 (15.6 ng/ml), PDGF (12 pg/ml), NGF (<0.2 ng/ml), and TGF-β (2.3 ng/ml). In gfrMG, however, the levels of these factors (except for TGF-β) are significantly reduced (0–0.1 pg/ml FGF-2, <0.5 ng/ml EGF, 5 ng/ml IGF-1, <5 pg/ml PDGF, <0.2 ng/ml NGF, and 1.7 ng/ml TGF-β; manufacturer's data). Nonetheless, IGF-1 can promote proliferation of NPCs at 10–100 ng/ml (Aberg et al., 2003; Kalluri et al., 2007). Thus, although the concentration is low, IGF-1 might promote proliferation of NPCs. At 4 weeks, the

number of Ki67-positive proliferating cells was reduced, and there was no significant difference between grafts with or without gfrMG (Fig. 3D), suggesting that gfrMG did not enhance tumorigenesis and that most of the NPCs differentiated into astrocytes or postmitotic neurons.

When ES cell-derived NPCs were grafted into the brain with medium only, extensive invasion of CD45-positive leukocytes into the graft was observed after 24 hr. In contrast, only a small number of CD45-positive cells invaded gfrMG containing NPCs (Fig. 4A). These results suggest that gfrMG is able to protect grafted cells from exposure to cytotoxic cytokines such as IL-1β, IL-6, IFN-γ, and TNF-α secreted by inflammatory and immune cells (Mirza et al., 2004). Inflammatory or immune responses by the host brain inhibit neuronal differentiation of grafted NPCs (Ideguchi et al., 2008) or endogenous neural stem cells (Monje et al., 2003), an effect thought to be mediated by IL-6. Thus, early exposure of grafted NPCs to these cytokines could influence differentiation of the cells. In mice without immunosuppression, the number of TH-positive DA neurons per graft volume was significantly increased in the graft with gfrMG compared with that in the control graft (Fig. 2D). In contrast, the numbers did not differ significantly in mice with immunosuppression (Fig. 2E). Taken together, these data suggest that gfrMG promotes differentiation of DA neurons by preventing early exposure of grafted NPCs to cytokines such as IL-6.

As discussed above, our results suggest that the increase in the number of TH-positive cells in each graft is due not to direct induction of DA neuron differentiation by gfrMG but rather to its indirect effect and/or an increase in total cell number. In fact, in our in vitro experiment, gfrMG failed to generate significantly more TH-positive cells from 8-day SDIA colonies compared with other matrices (Fig. 1I). Because gfrMG contains 1.7 ng/ml TGF-β, which promotes differentiation of midbrain progenitors toward dopaminergic phenotype even at 1 ng/ml (Roussa et al., 2006), 8-day SDIA cells might not be mature enough to respond to TGF-β. Alternatively, the differentiation of DA neurons might be enhanced with longer observation, or the concentration of TGF-β in gfrMG might not be high enough to cause an effect in our system.

In conclusion, gfrMG is able to provide a suitable biological scaffold that creates a microenvironment for ES cell-derived NPCs. It supports cell survival and proliferation and protects NPCs from inflammatory or immune cells in vivo. Cell survival and differentiation can be enhanced by adding neurotrophic factors into the matrix (Loh et al., 2001). However, because MG is derived from mouse sarcomas, it cannot be used clinically owing to potential immunogenicity and pathogen transmission. For clinical applications, a human-derived matrix, such as the amniotic membrane that supports neural differentiation from ES cells (Ueno et al., 2006), plasma (Takenaga et al., 2007), or synthetic biomaterials must be developed.

REFERENCES

Aberg MAI, Aberg ND, Palmer TD, Alborn AM, Carlsson-Skwirut C, Bang P, Rosengren LE, Olsson T, Gage FH, Eriksson PS. 2003. IGF-I has a direct proliferative effect in adult hippocampal progenitor cells. Mol Cell Neurosci 24:23–40.

Bhang SH, Lim JS, Choi CY, Kwon YK, Kim BS. 2007. The behavior of neural stem cells on biodegradable synthetic polymers. J Biomater Sci Polym Ed 18:223–239.

Cao F, Sadrzadeh Rafie AH, Abilez OJ, Wang H, Blundo JT, Pruitt B, Zarins C, Wu JC. 2007. In vivo imaging and evaluation of different biomatrices for improvement of stem cell survival. J Tissue Eng Regen Med (in press).

Emgard M, Hallin U, Karlsson J, Bahr BA, Brundin P, Blomgren K. 2003. Both apoptosis and necrosis occur early after intracerebral grafting of ventral mesencephalic tissue: a role for protease activation. J Neurochem 86:1223–1232.

Freed CR, Greene PE, Breeze RE, Tsai WY, DuMouchel W, Kao R, Dillon S, Winfield H, Culver S, Trojanowski JQ, Eidelberg D, Fahn S. 2001. Transplantation of embryonic dopamine neurons for severe Parkinson's disease. N Engl J Med 344:710–719.

Frisch SM, Francis H. 1994. Disruption of epithelial cell–matrix interactions induces apoptosis. J Cell Biol 124:619–626.

Gelain F, Bottai D, Vescovi A, Zhang S. 2006. Designer self-assembling Peptide nanofiber scaffolds for adult mouse neural stem cell 3-dimensional cultures. PLoS ONE 1:e119.

Goldman S. 2005. Stem and progenitor cell-based therapy of the human central nervous system. Nat Biotechnol 23:862–871.

Hubert T, Grimal S, Carroll P, Fichard-Carroll A. 2008. Collagens in the developing and diseased nervous system. Cell Mol Life Sci [E-pub ahead of print].

Ideguchi M, Shinoyama M, Gomi M, Hayashi H, Hashimoto N, Takahashi J. 2008. Immune or inflammatory response by the host brain suppresses neuronal differentiation of transplanted ES cell-derived neural precursor cells. J Neurosci Res (in press).

Kalluri HSG, Vemuganti R, Dempsey RJ. 2007. Mechanism of insulin-like growth factor I-mediated proliferation of adult neural progenitor cells: role of Akt. Eur J Neurosci 25:1041–1048.

Kawasaki H, Mizuseki K, Nishikawa S, Kaneko S, Kuwana Y, Nakanishi S, Nishikawa S, Sasai Y. 2000. Induction of midbrain dopaminergic neurons from ES cells by stromal cell-derived inducing activity. Neuron 28:31–40.

Kerever A, Schnack J, Vellinga D, Ichikawa N, Moon C, Arikawa-Hirasawa E, Efird JT, Mercier F. 2007. Novel extracellular matrix structures in the neural stem cell niche capture the neurogenic factor fibroblast growth factor 2 from the extracellular milieu. Stem Cells 25:2146–2157.

Kleinman HK, McGarvey ML, Hassell JR, Star VL, Cannon FB, Laurie GW, Martin GR. 1986. Basement-membrane complexes with biological-activity. Biochemistry (Moscow) 25:312–318.

Kurosaka K, Takahashi M, Watanabe N, Kobayashi Y. 2003. Silent cleanup of very early apoptotic cells by macrophages. J Immunol 171:4672–4679.

Kutschka I, Chen IY, Kofidis T, Arai T, von Degenfeld G, Sheikh AY, Hendry SL, Pearl J, Hoyt G, Sista R, Yang PC, Blau HM, Gambhir SS, Robbins RC. 2006. Collagen matrices enhance survival of

transplanted cardiomyoblasts and contribute to functional improvement of ischemic rat hearts. Circulation 114:I167–I173.

Lelievre SA, Weaver VM, Nickerson JA, Larabell CA, Bhaumik A, Petersen OW, Bissell MJ. 1998. Tissue phenotype depends on reciprocal interactions between the extracellular matrix and the structural organization of the nucleus. Proc Natl Acad Sci U S A 95:14711–14716.

Lindvall O, Kokaia Z, Martinez-Serrano A. 2004. Stem cell therapy for human neurodegenerative disorders—how to make it work. Nat Med: S42–S50.

Loh NK, Woerly S, Bunt SM, Wilton SD, Harvey AR. 2001. The regrowth of axons within tissue defects in the CNS is promoted by implanted hydrogel matrices that contain BDNF and CNTF producing fibroblasts. Exp Neurol 170:72–84.

Lutolf MP, Hubbell JA. 2005. Synthetic biomaterials as instructive extracellular microenvironments for morphogenesis in tissue engineering. Nat Biotechnol 23:47–55.

Ma W, Tavakoli T, Derby E, Serebryakova Y, Rao MS, Mattson MP. 2008. Cell-extracellular matrix interactions regulate neural differentiation of human embryonic stem cells. BMC Dev Biol 8(90).

Matsuura R, Kogo H, Ogaeri T, Miwa T, Kuwahara M, Kanai Y, Nakagawa T, Kuroiwa A, Fujimoto T, Torihashi S. 2006. Crucial transcription factors in endoderm and embryonic gut development are expressed in gut-like structures from mouse ES cells. Stem Cells 24:624–630.

Mirza B, Krook H, Andersson P, Larsson LC, Korsgren O, Widner H. 2004. Intracerebral cytokine profiles in adult rats grafted with neural tissue of different immunological disparity. Brain Res Bull 63:105–118.

Monje ML, Toda H, Palmer TD. 2003. Inflammatory blockade restores adult hippocampal neurogenesis. Science 302:1760–1765.

Nishino H, Hida H, Takei N, Kumazaki M, Nakajima K, Baba H. 2000. Mesencephalic neural stem (progenitor) cells develop to dopaminergic neurons more strongly in dopaminergic-depleted striatum than in intact striatum. Exp Neurol 164:209–214.

Ogawa K, Saito A, Matsui H, Suzuki H, Ohtsuka S, Shimosato D, Morishita Y, Watabe T, Niwa H, Miyazono K. 2007. Activin-nodal signaling is involved in propagation of mouse embryonic stem cells. J Cell Sci 120:55–65.

Olanow CW, Goetz CG, Kordower JH, Stoessl AJ, Sossi V, Brin MF, Shannon KM, Nauert GM, Perl DP, Godbold J, Freeman TB. 2003. A double-blind controlled trial of bilateral fetal nigral transplantation in Parkinson's disease. Ann Neurol 54:403–414.

Patino M, Neiders M, Andreana S, Noble B, Cohen R. 2002a. Collagen as an implantable material in medicine and dentistry. J Oral Implantol 28:220–225.

Patino M, Neiders M, Andreana S, Noble B, Cohen R. 2002b. Collagen: an overview. Implant Dent 11:280–285.

Qian LC, Saltzman WM. 2004. Improving the expansion and neuronal differentiation of mesenchymal stem cells through culture surface modification. Biomaterials 25:1331–1337.

Roussa E, Wiehle M, Dunker N, Becker-Katins S, Oehlke O, Krieglstein K. 2006. Transforming growth factor beta is required for differentiation of mouse mesencephalic progenitors into dopaminergic neurons in vitro and in vivo: ectopic induction in dorsal mesencephalon. Stem Cells 24:2120–2129.

Sortwell CE, Pitzer MR, Collier TJ. 2000. Time course of apoptotic cell death within mesencephalic cell suspension grafts: Implications for improving grafted dopamine neuron survival. Exp Neurol 165:268–277.

Takenaga M, Ohta Y, Tokura Y, Hamaguchi A, Suzuki N, Nakamura M, Okano H, Igarashi R. 2007. Plasma as a scaffold for regeneration of neural precursor cells after transplantation into rats with spinal cord injury. Cell Transplant 16:57–65.

Tisay KT, Key B. 1999. The extracellular matrix modulates olfactory neurite outgrowth on ensheathing cells. J Neurosci 19:9890–9899.

Ueno M, Matsumura M, Watanabe K, Nakamura T, Osakada F, Takahashi M, Kawasaki H, Kinoshita S, Sasai Y. 2006. Neural conversion of ES cells by an inductive activity on human amniotic membrane matrix. Proc Natl Acad Sci U S A 103:9554–9559.

Weinand C, Gupta R, Huang AY, Weinberg E, Madisch I, Qudsi RA, Neville CM, Pomerantseva I, Vacanti JP. 2007. Comparison of hydrogels in the in vivo formation of tissue-engineered bone using mesenchymal stem cells and beta-tricalcium phosphate. Tissue Eng 13: 757–765.

Xiao QZ, Zeng LF, Zhang ZY, Margariti A, Ali ZA, Channon KM, Xu QB, Hu YH. 2006. Sca-1$^+$ progenitors derived from embryonic stem cells differentiate into endothelial cells capable of vascular repair after arterial injury. Arterioscler Thromb Vasc Biol 26:2244–2251.

Xu G, Nie DY, Wang WZ, Zhang PH, Shen J, Ang BT, Liu GH, Luo XG, Chen NL, Xiao ZC. 2004. Optic nerve regeneration in polyglycolic acid-chitosan conduits coated with recombinant L1-Fc. Neuroreport 15:2167–2172.

Yang F, Murugan R, Ramakrishna S, Wang X, Ma YX, Wang S. 2004. Fabrication of nano-structured porous PLLA scaffold intended for nerve tissue engineering. Biomaterials 25:1891–1900.

Yoshino JE, Neuberger TJ, Cornbrooks CJ, Tennekoon GI, Eng LF, Devries GH. 1990. Proliferation and differentiation of a transfected schwann-cell line is altered by an artificial basement-membrane. Glia 3: 315–321.

Zawada WM, Zastrow DJ, Clarkson ED, Adams FS, Bell KP, Freed CR. 1998. Growth factors improve immediate survival of embryonic dopamine neurons after transplantation into rats. Brain Res 786:96–103.

Zhang PC, Zhang H, Wang H, Wei YJ, Hu SS. 2006. Artificial matrix helps neonatal cardiomyocytes restore injured myocardium in rats. Artif Organs 30:86–93.
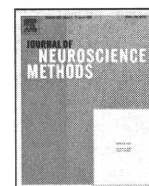
Objective and quantitative evaluation of motor function in a monkey model of Parkinson's disease

Hidemoto Saiki [a,b,c,1], Takuya Hayashi [d,1], Ryosuke Takahashi [b], Jun Takahashi [c,*]

[a] Department of Neurology, Kitano Hospital, The Tazuke Kofukai Medical Research Institute, Osaka, Japan
[b] Department of Neurology, Kyoto University Graduate School of Medicine, Kyoto, Japan
[c] Department of Biological Repair, Institute for Frontier Medical Sciences, Kyoto University, 53 Shogoin Kawahara-cho, Sakyo-ku, Kyoto 606-8507, Japan
[d] Functional Probe Research Laboratory, RIKEN Center for Molecular Imaging Science, Kobe, Japan

ABSTRACT

Monkeys treated with 1-methyl-4-phenyl-1,2,5,6-tetrahydropyridine (MPTP) are currently the best animal model for Parkinson's disease (PD) and have been widely used for physiological and pharmacological investigations. However, objective and quantitative assessments have not been established for grading their motor behaviors. In order to develop a method for an unbiased evaluation, we performed a video-based assessment, used qualitative rating scales, and carried out an *in vivo* investigation of dopamine (DA) transporter binding in systemically MPTP-treated monkeys. The video-based analysis of spontaneous movement clearly demonstrated a significant correlation with the qualitative rating score. The assessment of DA transporter (DAT) function by [^{11}C]-CFT-PET showed that, when compared with normal animals, the MPTP-treated animals exhibited decreased CFT binding in the bilateral striatum, particularly in the dorsal part in the putamen and caudate. Among the MPTP-treated monkeys, an unbiased PET analysis revealed a significant correlation between CFT binding in the midbrain and qualitative rating scores or the amount of spontaneous movements. These results indicate that a video-based analysis can be a reliable tool for an objective and quantitative evaluation of motor dysfunction of MPTP-treated monkeys, and furthermore, that DAT function in the midbrain may also be important for the evaluation.

© 2010 Elsevier B.V. All rights reserved.

1. Introduction

In rodents, non-human primates, and humans, systemic administration of 1-methyl-4-phenyl-1,2,5,6-tetrahydropyridine (MPTP) causes the selective loss of dopamine (DA) neurons in the substantia nigra (SN), as seen in patients with Parkinson's disease (PD). The treatment of monkeys with MPTP has become the most successful primate model of human neurodegenerative disease. This treatment evokes a persistent syndrome in the monkey and produces virtually all of the cardinal behavioral, biochemical, and histological changes that occur within the DA system in PD (Andersson et al., 2006; Burns et al., 1983). Furthermore, most of the current anti-parkinsonism therapies were tested for efficacy and approved based on this model. Thus, MPTP-treated animals have been contributing to physiological and pharmacological investigations as PD models (Jenner, 2003).

A number of qualitative rating scales have been employed to evaluate the neurological functions of MPTP-treated monkeys.

These scales, however, are functions of multiple variables, and the impact on each variable differs among the scales (Imbert et al., 2000). Therefore, more objective evaluation methods are needed for an accurate comparison of the effects of anti-parkinsonism therapies. Previous studies have used a video-based analysis system as a qualitative assessment of behavioral evaluations of rodents and non-human primates (Chassain et al., 2001; Liu et al., 2009; Togasaki et al., 2005). This type of system provides qualitative interpretations of movement, or the measurement of specific actions, as well as a quantitative assessment. Thus, the first aim of this study was to validate a video-based movement analysis system by comparing its results with behavioral evaluation using a qualitative rating scale.

An objective evaluation for indicating the function of the DA system can be also obtained using neuroimaging techniques. Specifically, positron emission tomography (PET) using 6-[^{18}F]-fluoro-3,4-dihydroxy-L-phenylalanine ([^{18}F]-F-DOPA), [^{11}C]-2β-carbomethoxy-3β-(4-fluorophenyl)-tropane ([^{11}C]-CFT), and [^{11}C]-raclopride has been clinically used to evaluate DA synthesis capacity, DA transporter (DAT), and DA receptors, respectively. Several PET studies in humans (Bruck et al., 2009; Nurmi et al., 2003; Rinne et al., 2001) and monkeys (Oiwa et al., 2003; Wullner et al., 1994) have demonstrated a behavior-related decrease in DA

---

synthesis or DAT density in the striatum. However, the behavioral evaluations that were used were not fully established as objective, and the anatomical focus of these studies was the striatum, where DA and DAT are most abundant. Thus, the second aim of this study was to investigate a correlation between the whole brain PET analysis and the behavior evaluations. In particular, we focused on DAT as an indicator of DA function, because it has been reported that CFT-PET is more sensitive than F-DOPA-PET in detecting DA hypofunction (Forsback et al., 2004). The DAT is a protein localized on the presynaptic membrane of DA neuron terminals; it clears DA from the interstitial space back into presynaptic elements by a process of facilitated diffusion (Kuhar et al., 1990). In addition, several studies have shown that a substantial amount of DAT also localizes in the somatodendritic membrane of DA neurons (Cheramy et al., 1981; Cobb and Abercrombie, 2002; Timmerman and Abercrombie, 1996) where it modulates local DA transmission within the SN (Vandecasteele et al., 2008) and thus may have a distinct role from that of nigro-striatal DA (Cheramy et al., 1981).

To accomplish these aims, we evaluated the neurological functions of MPTP-treated monkeys using a qualitative rating scale and video-based analysis system. We then performed an unbiased voxel-based analysis of the whole brain using [^{11}C]-CFT-PET.

2. Methods

2.1. Animals

Adult (4 y.o.) cynomolgus monkeys (*Macaca fascicularis*), weighing 3.3–4.0 kg, were provided by Shin Nippon Biomedical Laboratories, Ltd., Kagoshima, Japan for this study. Animals in the MPTP-treated group ($n = 13$) were given intravenous injections of MPTP HCl (0.4 mg/kg as free base, Sigma–Aldrich) twice a week until persistent parkinsonian behavioral disturbances, such as tremor, bradykinesia, and impaired balance, became evident. The animals received an average of 15.6 MPTP administrations, and those that presented stable parkinsonism for over 12 weeks were used for the experiments. We also used normal monkeys for the [^{11}C]-CFT-PET study ($n = 5$) and for behavioral estimation ($n = 8$). Monkeys were cared for and handled according to the Guidelines for Animal Experiments of Kyoto University and the National Institute of Health Guide for the Care and Use of Laboratory Animals (NIH Publications No. 80-23) revised 1996.

2.2. Qualitative rating scale

The behavior of the animals was evaluated according to a rating scale for monkey PD models (Takagi et al., 2005). This scale rates nine items: alertness (0–2); head checking movement (0–2); eye blinking and movement (0–2); posture (0–3); balance (0–3); motility at rest (0–3); reactive motility to external stimuli (0–3); walking (0–3); and tremor (0–3). Normal and minimum score is 0, and maximum total score is 24. The evaluation was performed by a well-trained examiner who was not involved in the video-based behavior analysis.

2.3. Spontaneous movement assessment

A mini-DV camcorder (SONY DCR-TRV 50) was placed in front of the monkey cage, which recorded spontaneous movements of the animals for 20 min (with nobody in the room). The video records were analyzed by a Vigie Primate video-based analysis system (View Point, Lyon, France (Chassain et al., 2001; Liu et al., 2009)). The images were digitized with a 720 × 480 pixel definition on 256 gray levels according to the NTSC TV standard, and the changes in pixels from one image to the next were counted every 66.67 ms.

2.4. Statistical analysis for behavior

The amount of spontaneous behavior was analyzed by a Student's *t*-test between groups (MPTP vs. normal group). A linear regression analysis was applied for a correlation analysis between the clinical rating score and counts of spontaneous movement. We further analyzed the pattern of movements in the spontaneous behaviors by repeated ANOVA. A post hoc Bonferroni analysis was used to compare among groups of monkeys with different severities of MPTP-induced parkinsonism. We considered *p*-values less than 0.05 as significant. For the repeated ANOVA, a Huynh–Feldt adjustment was applied to *p*-values when Mauchy's sphericity test was significant.

2.5. [^{11}C]-CFT-PET scan

Eight of the MPTP-treated animals (of 13) and five normal animals were used for a PET study. For the scan, the animals were placed under general anesthesia with a continuous intravenous infusion of propofol (6 mg/kg/h), and their respiration state was adjusted to normal range (PaO$_2$ > 100 mmHg, PaCO$_2$ ~35 mmHg) by altering the ventilation rate. The PET scan was started 2 h after achieving a physiologically stable state. After a transmission scan using a ^{68}Ge/^{68}Ga rod source for attenuation correction, a mean of 187 MBq of [^{11}C]-CFT was injected at the start of a 2D dynamic PET scan lasting 60 min (10 s × 18, 30 s × 6, 120 s × 7, 300 s × 8). The PET scan was performed on an ECAT EXACT HR+ PET scanner (Siemens-CTI, Knoxville, USA). The images were reconstructed using a filtered back projection algorithm with a Gaussian filter size of 2 mm. On different days, we obtained 3D T1-weighted magnetic resonance images (MRI) for co-registration and structural normalization for each animal (IR-FSPGR, TR = 9.4 ms, TE = 2.1 ms, TI = 600 ms) using a 3T MRI scanner (Signa LX VAH/I, GE, Milwaukee, USA).

2.6. PET data analysis

Dopamine transporter binding in the brain was quantified voxel-by-voxel as a binding potential (BP$_{ND}$) image, based on the simplified reference tissue model (Gunn et al., 1997). The reference region was defined in the cerebellum by delineating the boundary on a T1-weighted image that was pre-registered to the time-integrated PET image, and the time-radioactivity curve obtained in the reference region was used to calculate the binding potential image. We calculated a tracer delivery image (RI image), which was used for the next step of co-registration between PET and MRI images.

2.7. Registration across modalities (PET, MRI) and to the standard space

Before registration, non-brain structures were removed from MRI and PET images using Brain Extraction Tools in FSL (Smith, 2002). Then, for each subject, all of the MRI images were realigned to the T1 image by rigid body transformation (using FLIRT). The T1-weighted image was transformed to the standard space of a *Macaque fascicularis* brain (Hayashi et al., 2004) by affine transformation. This transformation matrix was then applied to all the MRI and PET data to be analyzed in the same standard space across modalities and individuals.

2.8. Voxel-based statistics of BP$_{ND}$ images of [^{11}C]-CFT

The voxel-based statistics of BP$_{ND}$ images of [^{11}C]-CFT were carried out using FEAT Version 5.98, part of FSL (FMRIB's Software Library). The following pre-statistics processing was applied to each

image: co-registration between subjects' PET-BP$_{ND}$ images using FLIRT (FMRIB's linear image registration toolkit) followed by spatial smoothing using a Gaussian kernel of FWHM 4.0 mm. When needed, we also scaled the voxel-based maps of BP$_{ND}$ to the global mean value in the entire brain volume. Statistical analysis was carried out using FILM without temporal filtering. For comparison between normal and MPTP-treated animals, we estimated the contrast of the group effect in BP$_{ND}$ images. For correlation analysis of BP$_{ND}$ images with behavioral estimations, both the qualitative rating scale (ranging from 4 to 11) and spontaneous movement scores (ranging 12–161.2) were de-meaned (i.e., subtracted by each mean value) and separately entered into the design matrices for statistical analysis. Z-statistic (Gaussianized T/F) images were thresholded using clusters determined by $Z > 2.3$, and were assigned a (corrected) cluster significance threshold of $p = 0.05$ (Worsley, 2001). We also performed an analysis of the regions of interest (ROI) at the putamen, caudate, ventral striatum and SN. The obtained BP$_{ND}$ values were plotted against each group, region, and side. An ANOVA was also performed with the following factors: region, group, side, and the interaction terms. To demonstrate a correlation between BP$_{ND}$ values and behavioral estimations, BP$_{ND}$ values, derived from the voxel having the most significant effect in the voxel-based correlation analysis, were plotted against the behavioral estimations.

3. Results

3.1. Behavioral evaluation

The video-based analysis demonstrated that the amount of spontaneous movement was significantly less (an 88% reduction) in the MPTP-treated monkeys compared to normal monkeys [Fig. 1A; $t(20) = 5.2$, $p < 0.01$]. The parkinsonian monkeys were then divided into three groups by qualitative rating scores; mildly affected: less than 5 points ($n = 4$); moderately affected: 5–9 points ($n = 4$); severely affected: more than 10 points ($n = 5$). When analyzed by ANOVA, we found that the extent of spontaneous movement was significantly different among these three groups ($F(2,10) = 29.3$, $p < 0.001$) and post hoc multiple paired comparison disclosed a significant group difference between mildly vs. moderately affected groups ($p < 0.01$, Turkey HSD); moderately vs. severely affected ($p < 0.01$); and mildly vs. severely affected ($p < 0.001$) (Fig. 1B). The extent of movement score was negatively correlated with qualitative rating scores ($y = -12.2x + 170.1$, $R^2 = 0.792$, $t_{24} = -6.48$, $p < 0.0001$; Fig. 1C). For further investigation of the altered movement patterns in the parkinsonian monkeys, we classified the size of the movements into four levels by the amount of pixel changes (large: over 501 pixels per 66.67 ms; medium: 101–500 pixels; small: 11–100 pixels; no movement: less than 10 pixels), and the total time for each level of movements was counted for each monkey group, including normal monkeys. A repeated ANOVA (with factors of movement size, group, and interaction terms) revealed significant effects of movement size ($F(2.1, 36.2) = 71.3$, $p < 0.001$), an interaction of movement size and group ($F(6.4, 36.2) = 30.3$, $p < 0.001$), but there were no significant affects of group ($F(3,17) = 0.68$, $p = 0.58$) on the amount of pixel changes; this suggests that the movement types differed by group. As shown in Fig. 2A, the period of medium- and large-sized movements decreased according to the severity of neurological symptoms in the MPTP-treated monkeys. However, the period of small movements significantly increased ($p < 0.001$) whereas the non-movement period decreased in mildly affected models of parkinsonism ($p < 0.05$) compared to those in normal monkeys. A visual rating of the video records revealed that normal monkeys exhibited large movements like climbing and jumping, while severely affected models remained almost still. In the most mildly
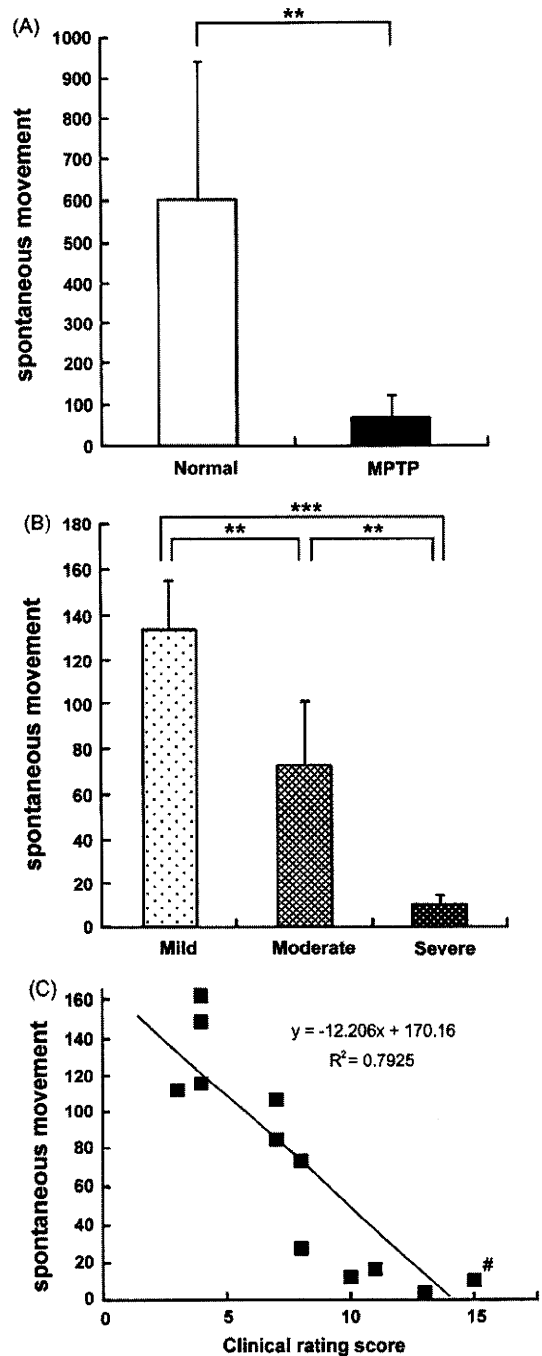

Fig. 1. Correlation between neurological score and spontaneous movement. (A) Spontaneous movement (pixel changes/66.67 ms) of normal ($n = 8$) and MPTP-treated monkeys ($n = 13$). (B) Comparison of spontaneous movement between mild ($n = 4$), moderate ($n = 4$), and severe ($n = 5$) models. Data are presented as the means $\pm$ SD. **$p < 0.01$, ***$p < 0.001$, Turkey HSD. (C) The plot of each sample. ($n = 13$). #Two values are too close to distinguish on the graph (score = 15, pixel change = 10.6; score = 15, pixel change = 11.0).

affected animals, both resting and postural hand tremor were shown in the video, and the raw data analysis of pixel changes revealed a sequential pattern of 10–30 pixel changes with 5–6 Hz periodicity (Fig. 2B). These results suggest that video-based analysis can provide objective quantification of monkey's movements that correlate with other behaviors such as posture and balance.
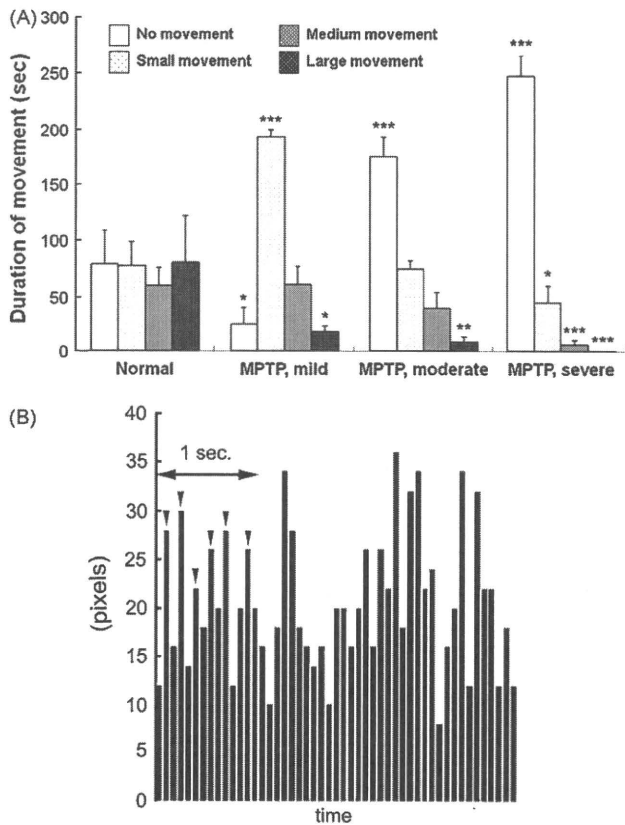
Fig. 2. Assessment of movement patterns in MPTP-treated monkeys. (A) Total duration of movement in normal and model monkeys. Data are presented as the means ± SD. Each value was compared with the one of normal monkeys. *$p < 0.05$, **$p < 0.01$, ***$p < 0.001$. (B) Representative pixel changes per each time unit (66.67 ms) in the mildly affected monkey.

Fig. 3. Group comparison of [^{11}C]-CFT BP$_{ND}$ revealed by PET. (A) Voxel-based statistical results of group comparison between normal and MPTP-treated monkeys. Significant cluster ($Z > 2.3$, corrected $p < 0.05$) was found in the contrast of (normal > MPTP-treated), indicating decrease of CFT BP$_{ND}$. The maximal Z score was found in the right putamen (crosshair). (B) Bar plot of BP$_{ND}$ values obtained by region of interest (ROI) analysis. Simple group comparison of BP$_{ND}$ values for each region showed significant decrease in BP$_{ND}$ in the putamen (Put), caudate (Cau), ventral striatum (VS) and substantia nigra (SN) for both side (L, left; R, right). *$p < 0.05$, ***$p < 0.001$.

3.2. DAT function

In a PET analysis for DAT function, we first performed group comparisons between normal and MPTP-treated animals. A notably high binding of [^{11}C]-CFT was observed in the striatum in normal monkeys; this binding was much reduced in the MPTP-treated animals, particularly in the dorsal striatum. Voxel-based statistics for group comparison without performing the multiplicative mean voxel-value normalization revealed that the binding potential (BP) significantly decreased in a cluster involving the putamen and caudate nucleus, but mostly spared the rostro-ventral part of the striatum (Fig. 3A). The BP$_{ND}$ values in the ROI analysis are shown in Fig. 3B. A repeated ANOVA revealed significant effects of group ($F(1,11) = 80.3$, $p < 0.001$), the interaction of regions and groups ($F(2,22) = 16.2$, $p < 0.001$) and a marginal effect of regions ($F(1.3,14.3) = 3.28$, Huyn–Feldt adjusted, $p = 0.083$), but no significant effect of side ($F(1,11) = 0.31$, $p = 0.6$) on the BP values. In fact, the subsequent comparison of the group (normal vs. MPTP) for each region (including left and right side) disclosed a smaller decrease of [^{11}C]-CFT BP$_{ND}$ in the ventral striatum (-44% difference in mean values, $T(24) = 8.36$, $p < 0.001$) than in the dorsal striatum (caudate: -85%, $T(24) = 11.1$, $p < 0.001$, putamen: -72%, $T(24) = 12.2$, $p < 0.001$) (Fig. 3B).

We performed a voxel-based correlation analysis between [^{11}C]-CFT BP$_{ND}$ and spontaneous movements as well as qualitative rating scores in the MPTP-treated monkeys. We note that this was an unbiased analysis, i.e., a voxel-based comparison throughout the entire brain volume. Without multiplicative mean BP$_{ND}$ value normalization (i.e., quantitative BP$_{ND}$ images were used "as is" in the
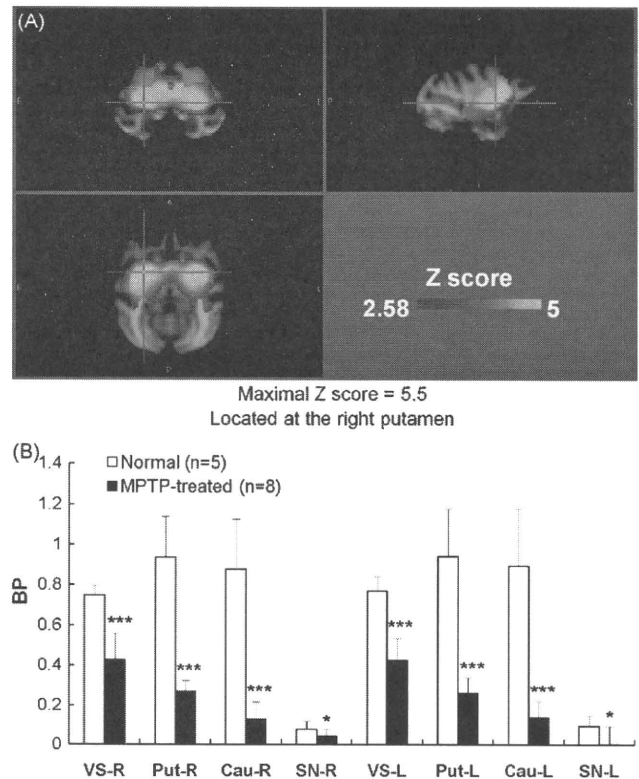
statistical analysis), there were no significant voxels or clusters in the voxel-based correlation analysis, either for qualitative rating score or spontaneous movement. We then applied multiplicative mean voxel-value normalization before the statistical analysis and found a significant cluster located in the midbrain for both qualitative rating score (Fig. 4A) and spontaneous movement (Fig. 5A); however, there was no significant difference in the striatal voxels as expected. With the BP$_{ND}$ values plotted, we found a negative correlation in the midbrain for qualitative rating score (Fig. 4B) and a positive correlation for spontaneous movement (Fig. 5B). These results suggest that neurological symptoms of MPTP-treated monkeys are more related to the DAT density in the midbrain than in the striatum.

4. Discussion

We showed that a video-based analysis system can detect a difference in spontaneous movements between normal and MPTP-treated monkeys. Moreover, we clearly showed a significant correlation between the quantity of spontaneous movements and the severity of qualitative rating scores. These results are consistent with previous studies which found a significant correlation of rating scale and the residual dopaminergic neurons in post-mortem evaluation (Elsworth et al., 2000). Other studies in clinical patients also found similar relationships between a DAT binding ligand and a clinical rating scale (UPDRS) in PD patients (Marek et al., 2001; Seibyl et al., 1995).
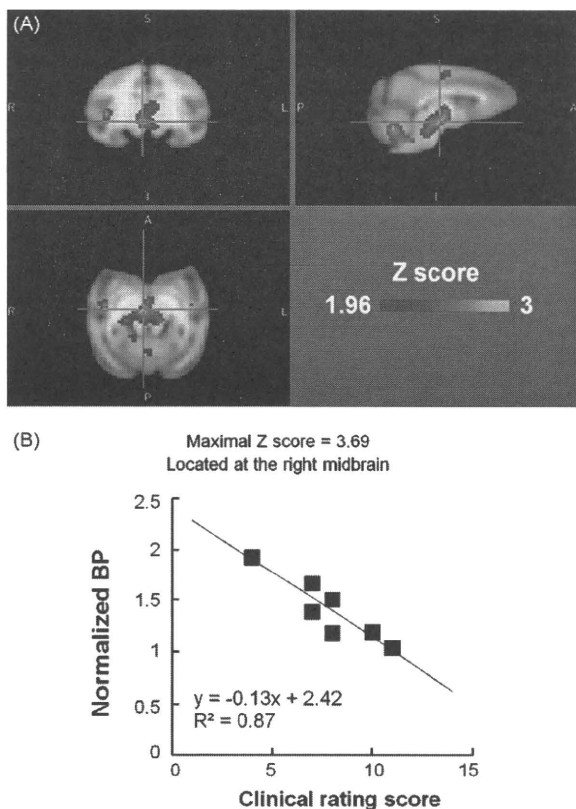
Fig. 4. Correlation analysis of [^{11}C]-CFT BP$_{ND}$ with qualitative rating score. (A) Voxel-based statistical results of correlation with qualitative rating score. Significant cluster ($Z > 2.3$, corrected $p < 0.05$) was found in the contrast of negative correlation with qualitative rating score. The maximal Z score was found in the right midbrain, close to the right substantia nigra (crosshair). (B) The plot of the normalized BP$_{ND}$ values at the right midbrain voxel with the maximal Z score in A.

Fig. 5. Correlation analysis of [^{11}C]-CFT BP$_{ND}$ with spontaneous movement. (A) Voxel-based statistical results of correlation with qualitative rating score. Significant cluster ($Z > 2.3$, corrected $p < 0.05$) was found in the contrast of positive correlation with video-based spontaneous behavior. The maximal Z score was located in the left midbrain, close to the left substantia nigra (crosshair). (B) The plot of the normalized BP$_{ND}$ values at the left midbrain voxel with the maximal Z score in A.

It has recently been reported that bradykinesia and rigidity were closely related, and that these items showed weaker correlations with other items such as freezing and tremor (van Rooden et al., 2009). This suggests that the component variables in a qualitative rating scale are not independent. Therefore, the correlation in this study seems reasonable. In fact, other video-based analyses of an acute phase (3–4 weeks) of MPTP-treatment with squirrel monkeys (Togasaki et al., 2005) or hemiparkinsonian cynomolgus monkeys (Liu et al., 2009) demonstrated a significant correlation between spontaneous movements and qualitative rating scores. In this study, we showed this correlation with a more chronic (more than 12 weeks) phase of a cynomolgus monkey model by systemic MPTP-treatment. Since the qualitative rating scores can be observer-dependent and may not be parametric evaluations if not properly categorized (see below), the video-based analysis can be a reliable tool for the objective quantification of motor function.

The qualitative rating scale used in the present study has potential drawbacks. It principally includes items that may not necessarily be specific to PD symptoms (alertness, head checking movement), and it would tend to exaggerate the behavioral change due to the overlap of similar items (for example, balance and walking). Because of the difficulty in verbal communication, there seem to be no perfect qualitative rating scale for monkey behaviors (Imbert et al., 2000), but our qualitative ratings scores may need to be optimized to increase the specificity and sensitivity to behavioral symptoms of PD model.

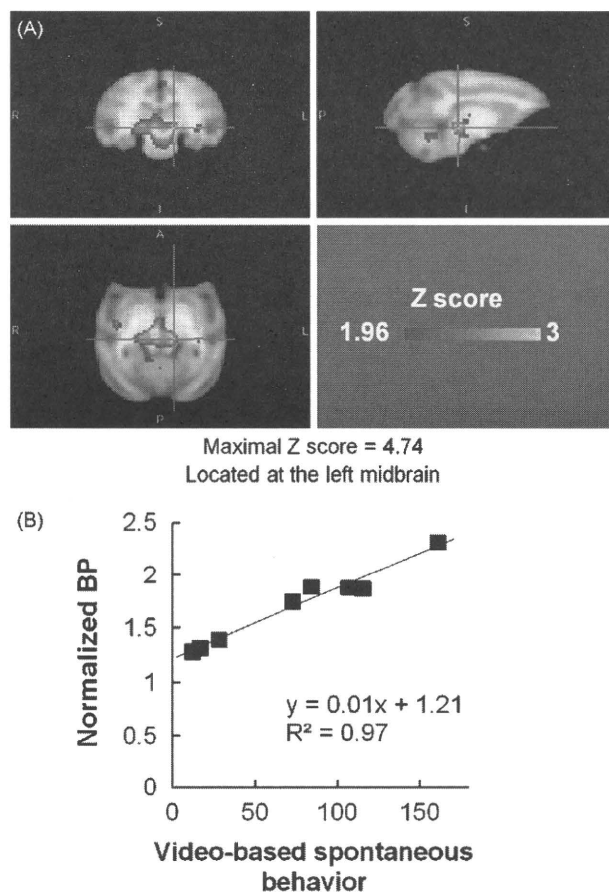In addition to a simple comparison between normal and MPTP-treated monkeys, we investigated the alteration of movement patterns between the mildly, moderately, and severely affected monkeys and found that mildly affected monkeys exhibited more small movements than normal monkeys. This may be due to an increase in resting and postural hand tremor in mildly affected animals. In fact, both resting and postural hand tremor, apparent on the video monitoring, exhibited an amplitude of 10–30 pixels and a frequency of 6 Hz. We would like to emphasize that the video-based analysis is able to distinguish tremor and count its frequency. In human patients, a large body of clinical data indicates that tremor is predominantly observed in early stage or mildly affected patients (Kang et al., 2005) and later with the progression of the disease, the increased akinesis or rigidity conceals the tremors. Consistent with this idea, it is often reported that appropriate administration of anti-parkinsonian medication leads to the reappearance of resting tremor in PD patients. In contrast, there is another argument that such tremor-dominant models are pathophysiologically different from other models in terms of their vulnerability to MPTP toxicity, since the disease of tremor-dominant PD is known to have a relatively benign course compared to the cases with marked bradykinesia (Jankovic and Kapadia, 2001). These ideas should be further explored by future studies, including, for example, the repeated assessment of behaviors during the progression of symptoms in the course of a MPTP-poisoning regimen or during long-term follow up.

Our PET study showed an extensive decrease of [^{11}C]-CFT BP$_{ND}$ in the striatum of the MPTP-treated monkeys, particularly in the dorsal region. This is consistent with previous studies on MPTP-treated monkeys (Brownell et al., 2003) and human PD patients (Nurmi et al., 2003; Rinne et al., 2001). The preferential depletion of DAT in the dorsal, rather than ventral striatum is also consistent with previous studies using PET (Doudet et al., 2006) and pathological assessment (Chiueh et al., 1985). More importantly, in our unbiased analysis through the whole brain of MPTP-treated animals, we found that [^{11}C]-CFT BP$_{ND}$ in the midbrain was significantly correlated with both of our behavioral assessments, suggesting that DA transmission in the midbrain is also involved in the deterioration of motor behaviors but shows a different correlation from that in the striatum. This finding is unexpected since a number of clinical studies in PD patients have shown a correlation of the degree of symptoms with the residual DA in the striatum. Since the current model animals were all in the chronic stage after systemic injection of MPTP, it may reflect the pathophysiology of advanced PD, in which compensatory changes occur in response to the degeneration of DA neurons.

We hypothesize that the midbrain DAT and DA might have a functional, compensatory role disparate from that in the striatum in MPTP-treated animals, when their striatal DA terminals were severely affected. The current animals all showed severely depleted DAT in the striatum, particularly in the motor-related area (i.e., putamen) of the striatum (~20% of normal animals). In addition, the current findings were obtained by the normalization of the global mean BP$_{ND}$ value, which removes variations in the residual CFT BP$_{ND}$ in the striatum from the BP$_{ND}$ values. In fact, the global mean BP$_{ND}$ values obtained here in MPTP-treated animals showed a highly significant correlation with the mean striatal BP$_{ND}$ values (Peason's correlation coefficient $r = 0.78$, $t_6 = 3.05$, $p < 0.05$), which were derived from the ROI covering the bilateral striatal areas. Thus, the results of the significant correlation between the midbrain BP$_{ND}$ and the behavioral assessments should depend on the level of DAT depletion in the striatum.

Accumulated evidence has suggested that somatodendritic DA release in SN has a distinct function other than nigro-striatal DA release (Cheramy et al., 1981; Cobb and Abercrombie, 2002; Robertson, 1992; Timmerman and Abercrombie, 1996). Observations in 6-hydroxydopamine (6-OHDA)-treated rats showed that CFT binding in the striatum reflected the number of nigral DA neurons more directly than that in the SN (Forsback et al., 2004), suggesting that DAT in the SN might be associated with a compensatory response to DA cell injuries. In another rodent study, the effect of DA depletion on motor performance was more evident when toxins were locally applied to SN than when applied to the striatum (Andersson et al., 2006). Taken together, our results suggest that changes in somatodendritic DAT in SN have a pivotal plastic function in motor performance, and that this function is distinct from the nigro-striatal DA system. Dendrites from the DA neurons located in SN pars compacta (SNc) extend throughout SN pars reticulata (SNr; (Prensa and Parent, 2001), and their release of DA has been shown to regulate the activity of the DA neurons themselves, the release of GABA from afferent fibers in SNr, and then the activity of its efferent projections (Cheramy et al., 1981; Robertson, 1992). Thus, our observations also support the pathophysiology of PD, where GABAergic output from SNr/internal segment of GP is a key controller of parkinsonian symptoms (DeLong, 1990). As to the functional role of DA transmission in the midbrain, future studies including pathological studies and other imaging modalities that can evaluate neuronal activity such as [^{18}F]-FDG PET or post-synaptic D1/D2 dopamine receptors should be performed.

In conclusion, in the current study with PD models in non-human primates, we showed that video-based analysis can be a reliable tool for an objective and quantitative evaluation of motor function. We also demonstrated that DAT function in the midbrain, not in the striatum, was correlated to the motor behaviors of the MPTP-treated monkeys, suggesting the functional segregation of midbrain DA release from striatal one.

Acknowledgments

References

Andersson DR, Nissbrandt H, Bergquist F. Partial depletion of dopamine in substantia nigra impairs motor performance without altering striatal dopamine neurotransmission. Eur J Neurosci 2006;24:617–24.

Brownell AL, Canales K, Chen YI, Jenkins BG, Owen C, Livni E, et al. Mapping of brain function after MPTP-induced neurotoxicity in a primate Parkinson's disease model. Neuroimage 2003;20:1064–75.

Bruck A, Aalto S, Rauhala E, Bergman J, Marttila R, Rinne JO. A follow-up study on 6-[^{18}F]fluoro-L-dopa uptake in early Parkinson's disease shows nonlinear progression in the putamen. Mov Disord 2009;24:1009–15.

Burns RS, Chiueh CC, Markey SP, Ebert MH, Jacobowitz DM, Kopin IJ. A primate model of parkinsonism: selective destruction of dopaminergic neurons in the pars compacta of the substantia nigra by N-methyl-4-phenyl-1,2,3,6-tetrahydropyridine. Proc Natl Acad Sci USA 1983;80:4546–50.

Chassain C, Eschalier A, Durif F. Assessment of motor behavior using a video system and a clinical rating scale in parkinsonian monkeys lesioned by MPTP. J Neurosci Methods 2001;111:9–16.

Cheramy A, Leviel V, Glowinski J. Dendritic release of dopamine in the substantia nigra. Nature 1981;289:537–42.

Chiueh CC, Burns RS, Markey SP, Jacobowitz DM, Kopin IJ. Primate model of parkinsonism: selective lesion of nigrostriatal neurons by 1-methyl-4-phenyl-1,2,3,6-tetrahydropyridine produces an extrapyramidal syndrome in rhesus monkeys. Life Sci 1985;36:213–8.

Cobb WS, Abercrombie ED. Distinct roles for nigral GABA and glutamate receptors in the regulation of dendritic dopamine release under normal conditions and in response to systemic haloperidol. J Neurosci 2002;22:1407–13.

DeLong MR. Primate models of movement disorders of basal ganglia origin. Trends Neurosci 1990;13:281–5.

Doudet DJ, Rosa-Neto P, Munk OL, Ruth TJ, Jivan S, Cumming P. Effect of age on markers for monoaminergic neurons of normal and MPTP-lesioned rhesus monkeys: a multi-tracer PET study. Neuroimage 2006;30:26–35.

Elsworth JD, Taylor JR, Sladek Jr JR, Collier TJ, Redmond Jr DE, Roth RH. Striatal dopaminergic correlates of stable parkinsonism and degree of recovery in old-world primates one year after MPTP treatment. Neuroscience 2000;95:399–408.

Forsback S, Niemi R, Marjamaki P, Eskola O, Bergman J, Gronroos T, et al. Uptake of 6-[^{18}F]fluoro-L-dopa and [^{18}F]CFT reflect nigral neuronal loss in a rat model of Parkinson's disease. Synapse 2004;51:119–27.

Gunn RN, Lammertsma AA, Hume SP, Cunningham VJ. Parametric imaging of ligand-receptor binding in PET using a simplified reference region model. Neuroimage 1997;6:279–87.

Hayashi T, Ohnishi T, Okabe S, Teramoto N, Nonaka Y, Watabe H, et al. Long-term effect of motor cortical repetitive transcranial magnetic stimulation [correction]. Ann Neurol 2004;56:77–85.

Imbert C, Bezard E, Guitraud S, Boraud T, Gross CE. Comparison of eight clinical rating scales used for the assessment of MPTP-induced parkinsonism in the Macaque monkey. J Neurosci Methods 2000;96:71–6.

Jankovic J, Kapadia AS. Functional decline in Parkinson disease. Arch Neurol 2001;58:1611–5.

Jenner P. The contribution of the MPTP-treated primate model to the development of new treatment strategies for Parkinson's disease. Parkinsonism Relat Disord 2003;9:131–7.

Kang GA, Bronstein JM, Masterman DL, Redelings M, Crum JA, Ritz B. Clinical characteristics in early Parkinson's disease in a central California population-based study. Mov Disord 2005;20:1133–42.

Kuhar MJ, Sanchez-Roa PM, Wong DF, Dannals RF, Grigoriadis DE, Lew R, et al. Dopamine transporter: biochemistry, pharmacology and imaging. Eur Neurol 1990;30(Suppl. 1):15–20.

Liu N, Yue F, Tang WP, Chan P. An objective measurement of locomotion behavior for hemiparkinsonian cynomolgus monkeys. J Neurosci Methods 2009;183:188–94.

Marek K, Innis R, van Dyck C, Fussell B, Early M, Eberly S, et al. [^{123}I]beta-CIT SPECT imaging assessment of the rate of Parkinson's disease progression. Neurology 2001;57:2089–94.

Nurmi E, Bergman J, Eskola O, Solin O, Vahlberg T, Sonninen P, et al. Progression of dopaminergic hypofunction in striatal subregions in Parkinson's disease using [^{18}F]CFT PET. Synapse 2003;48:109–15.

Oiwa Y, Eberling JL, Nagy D, Pivirotto P, Emborg ME, Bankiewicz KS. Overlesioned hemiparkinsonian non human primate model: correlation between clinical, neurochemical and histochemical changes. Front Biosci 2003;8:a155–66.

Prensa L, Parent A. The nigrostriatal pathway in the rat: a single-axon study of the relationship between dorsal and ventral tier nigral neurons and the strio-some/matrix striatal compartments. J Neurosci 2001;21:7247–60.

Rinne OJ, Nurmi E, Ruottinen HM, Bergman J, Eskola O, Solin O. [^{18}F]FDOPA and [^{18}F]CFT are both sensitive PET markers to detect presynaptic dopaminergic hypofunction in early Parkinson's disease. Synapse 2001;40:193–200.

Robertson HA. Dopamine receptor interactions: some implications for the treatment of Parkinson's disease. Trends Neurosci 1992;15:201–6.

Seibyl JP, Marek KL, Quinlan D, Sheff K, Zoghbi S, Zea-Ponce Y, et al. Decreased single-photon emission computed tomographic [^{123}I]beta-CIT striatal uptake correlates with symptom severity in Parkinson's disease. Ann Neurol 1995;38: 589–98.

Smith SM. Fast robust automated brain extraction. Hum Brain Mapp 2002;17: 143–55.

Takagi Y, Takahashi J, Saiki H, Morizane A, Hayashi T, Kishi Y, et al. Dopaminergic neurons generated from monkey embryonic stem cells function in a Parkinson primate model. J Clin Invest 2005;115:102–9.

Timmerman W, Abercrombie ED. Amphetamine-induced release of dendritic dopamine in substantia nigra pars reticulata: D1-mediated behavioral and elec-trophysiological effects. Synapse 1996;23:280–91.

Togasaki DM, Hsu A, Samant M, Farzan B, DeLanney LE, Langston JW, et al. The Webcam system: a simple, automated, computer-based video system for quan-titative measurement of movement in nonhuman primates. J Neurosci Methods 2005;145:159–66.

van Rooden SM, Visser M, Verbaan D, Marinus J, van Hilten JJ. Motor pat-terns in Parkinson's disease: a data-driven approach. Mov Disord 2009;24: 1042–7.

Vandecasteele M, Glowinski J, Deniau JM, Venance L. Chemical transmission between dopaminergic neuron pairs. Proc Natl Acad Sci USA 2008;105: 4904–9.

Worsley KJ. Statistical analysis of activation images. In: Jezzard P, Matthews PM, Smith SM, editors. Functional MRI: an introduction to methods. Oxford: Oxford University Press; 2001 (Chapter 14).

Wullner U, Pakzaban P, Brownell AL, Hantraye P, Burns L, Shoup T, et al. Dopamine terminal loss and onset of motor symptoms in MPTP-treated monkeys: a positron emission tomography study with ^{11}C-CFT. Exp Neurol 1994;126: 305–9.
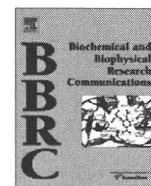
Mesenchymal stem cells cultured under hypoxia escape from senescence *via* down-regulation of p16 and extracellular signal regulated kinase

Yonghui Jin [a], Tomohisa Kato [a], Moritoshi Furu [a], Akira Nasu [a,b], Yoichiro Kajita [a,c], Hiroto Mitsui [a,d], Michiko Ueda [a], Tomoki Aoyama [e], Tomitaka Nakayama [b], Takashi Nakamura [b], Junya Toguchida [a,b,f,*]

[a] Department of Tissue Regeneration, Institute for Frontier Medical Sciences, Kyoto University, Japan
[b] Department of Orthopaedic Surgery, Graduate School of Medicine, Kyoto University, Japan
[c] Department of Urology, Graduate School of Medicine, Kyoto University, Japan
[d] Department of Musculoskeletal Medicine, Graduate School of Medical Sciences, Nagoya City University, Japan
[e] Human Health Sciences, Graduate School of Medicine, Kyoto University, Japan
[f] Center for iPS Cell Research and Application, Institute for Integrated Cell – Material Sciences, Kyoto University, Japan

ARTICLE INFO

ABSTRACT

Hypoxia has been considered to affect the properties of tissue stem cells including mesenchymal stem cells (MSCs). Effects of long periods of exposure to hypoxia on human MSCs, however, have not been clearly demonstrated. MSCs cultured under normoxic conditions (20% pO_2) ceased to proliferate after 15–25 population doublings, while MSCs cultured under hypoxic conditions (1% pO_2) retained the ability to proliferate with an additional 8–20 population doublings. Most of the MSCs cultured under normoxic conditions were in a senescent state after 100 days, while few senescent cells were found in the hypoxic culture, which was associated with a down-regulation of *p16* gene expression. MSCs cultured for 100 days under hypoxic conditions were superior to those cultured under normoxic conditions in the ability to differentiate into the chondro- and adipogenic, but not osteogenic, lineage. Among the molecules related to mitogen-activated protein kinase (MAPK) signaling pathways, extracellular signal regulated kinase (ERK) was significantly down-regulated by hypoxia, which helped to inhibit the up-regulation of *p16* gene expression. Therefore, the hypoxic culture retained MSCs in an undifferentiated and senescence-free state through the down-regulation of p16 and ERK.

© 2010 Published by Elsevier Inc.

Introduction

Mesenchymal stem cells (MSCs) are tissue stem cells with multi-directional differentiation potential, though molecular and cellular definitions remain controversial. At present, MSCs are defined as mononuclear adherent cells capable of differentiating into the osteo-, chondro-, and adipogenic lineages [1]. Despite the equivocal definition, the clinical application of MSCs to tissue regeneration and engineering has already been launched [2,3]. Like other tissue stem cells, MSCs have limited growth potential and cease to proliferate due to cellular senescence [4]. Cellular senescence is induced by both intrinsic and extrinsic factors [5]. The shortening of telomeres is the most important intrinsic factor, and mitogenic stimuli and DNA damage are main extrinsic factors. Oxidative stress caused by reactive oxygen species (ROS) is one of the factors inducing DNA damage [6]. Although cells with the

properties of MSCs have been isolated from adipose tissue [7], synovial tissue [8], and umbilical cord [9], bone marrow is the most frequent source of MSCs [10]. The oxygen concentration (pO_2) in bone marrow varies by the distance from the sinus ranging from 1% to 7% [11]. Therefore, although the precise location of MSCs in bone marrow is not known, the physiological oxygen concentration surrounding MSCs is much lower than the ambient oxygen concentration in cultures (20% pO_2). The high concentration of oxygen in standard culturing systems may produce excess oxidative stress, driving MSCs into a senescent state. Based on this concept, a number of studies have cultured MSCs under hypoxic conditions [12–17], and demonstrated that hypoxia is beneficial to the growth and also differentiation of MSCs, although the precise molecular mechanisms responsible for these phenotypic changes are not clear. The expression of the *p16* tumor suppressor gene is also important to cellular senescence [18,19]. We have shown that *p16* gene expression was gradually up-regulated during the life of MSCs *in vitro*, and tightly associated with the induction of cellular senescence [20]. Inhibition of *p16* gene expression by short interfering RNA for *p16* endowed senescent MSCs with the ability to re-proliferate and rescued them from senescence, indicating

the important role of p16 in the growth of MSCs [20]. A number of factors are involved in the up-regulation of *p16* gene expression *in vitro* including ROS [21].

Here we cultured MSCs long term (more than 200 days) under normoxic (20% pO_2) or hypoxic (1% pO_2) conditions, and compared growth profiles and the potential to differentiate into three lineages. We found that hypoxia increased the life span of MSCs by down-regulating *p16* gene expression and endowed superior properties for differentiation into the chondro-, and adipogenic lineages, which were associated with the down-regulation of extracellular signal regulated kinase (ERK).

Materials and methods

Primary cultured cells

The isolation of bone marrow-derived MSCs from donors was performed as described previously [22]. The Ethics Committee of the Faculty of Medicine, Kyoto University, approved the procedure and informed consent was obtained from each donor. Mononuclear cells containing MSCs were suspended in α-minimal essential medium with GlutaMAX (Invitrogen Co., Carlsbad, CA) supplemented with 10% fetal bovine serum (HyClone, South Logan, UT), 100 U/ml penicillin, and 100 mg/ml streptomycin, and separately cultured at a density of 2.5×10^5 cells/cm^2 under normoxic (20% pO_2 and 5% pCO_2) and hypoxic (1% pO_2 and 5% pCO_2) conditions at 37 °C. At 80% confluence, cells were collected, counted, and reseeded at a density of 3000 cells/cm^2. From this point, the number of population doublings (PD) was calculated based on the total cell number at each passage.

Senescence-associated-β-galactosidase assay

Cells were cultured on four-well chamber slides. The senescence-associated-β-galactosidase (SA-β-gal) assay was performed with a Senescence Detection Kit (BioVison, Mountain View, CA).

Induction of differentiation and quantitative evaluation

Differentiation was induced using standard methods [23], and evaluated quantitatively as follows.

Osteogenic differentiation. After 14 days, calcium deposits were visualized by alizarin red staining, and calcium content was quan-
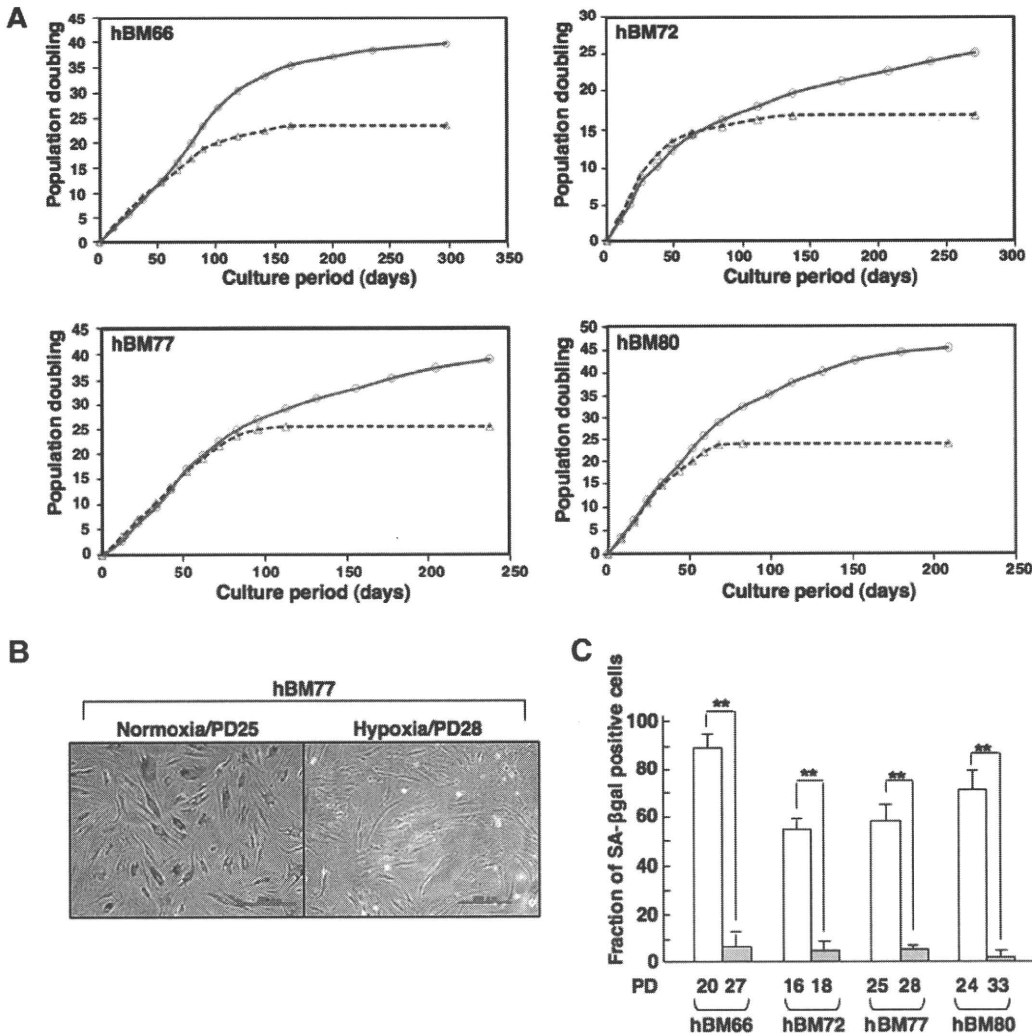

Fig. 1. Hypoxia extended the life span of MSCs *in vitro*. (A) Growth profiles of MSCs under normoxic (blue triangle) and hypoxic (red triangle) conditions. (B) Expression of SA-β-gal. hBM77 cells cultured for about 100 days under normoxic (PD25) or hypoxic (PD28) conditions were stained. (C) Quantitative analyses of SA-β-gal-positive cells among four hBM cell preparations at the indicated PD. White and gray box indicate normoxic and hypoxic conditions, respectively. (For interpretation of the references to color in this figure legend, the reader is referred to the web version of this paper.)

tified based on the OCPC method with a Calcium C-Test Wako Kit (Wako Pure Chemical Industries, Osaka, Japan).

Adipogenic differentiation. After 21 days, lipid-vacuoles were detected using Oil-Red-O staining, and the amount of triglyceride (TG) was quantified with a serum triglyceride kit (Sigma–Aldrich, St. Louis, MO). Protein content was quantified using BCA protein assay reagent (Pierce Biotechnology, Rockford, IL).

Chondrogenic differentiation. After 14 days, cartilage matrix was evaluated by alcian blue staining of cryosections, and the glycosaminoglycan (GAG) content in pellets was quantified with BLY-SCAN Dye and Dissociation reagents (BIOCOLOR, Belfast, UK). DNA content was quantified using a PicoGreen dsDNA Quantitation kit (Invitrogen, Carlsbad, CA).

Western blotting

Western blotting was performed as described [22]. The primary antibodies used were as follows: MAB1536 for HIF-1α, purchased from R&D Systems (Minneapolis, MN), and 551153 for p16, M12320 for ERK1, E23920 for phosphorylated ERK1/2, P19820 for p38, P39520 for phosphorylated p38, M54920 for pan-JNK, and S37220 for phosphorylated JNK, purchased from BD Biosciences Pharmingen (San Diego, CA). Blots were probed with horseradish peroxidase-conjugated goat anti-mouse IgG or goat anti-rabbit IgG (Santa Cruz Biotechnology, Santa Cruz, CA) and visualized using a chemiluminescence reagent ECL Plus Detection Kit (GE Healthcare UK Ltd., Little Chalfont, UK). The intensity of each band was calculated with Quantity One software, and evaluated as a ratio to that of control (β-actin).

Cell treatment

MAPK/ERK kinase (MEK) inhibitor treatment. Cells (2×10^5) were treated with U0126 (10 μM) (Promega, Madison, WI) for 96 h, and proteins were extracted every 24 h for Western blotting.

n-Propyl gallate (nPG) treatment. Cells (8×10^4) were treated with nPG (Sigma–Aldrich) at a concentration of 25–200 μM for 4 h, and proteins were extracted for Western blotting.

Statistical analyses

Statistical analyses were performed using Statcel software. Data were assessed using the Pearson product-moment correlation coefficient and Student's *t*-test.

Results

Hypoxia elongated growth of MSCs

MSCs were isolated from bone marrow of four donors, designated hBM66, hBM72, hBM77, and hBM80, respectively, and cultured under normoxic or hypoxic conditions as described in Materials and methods. In the case of hBM66, there was no significant difference between normoxic and hypoxic cultured-cells in terms of growth profile until PD15 (Fig. 1). After this stage, normoxic cultured-cells ceased to proliferate, whereas hypoxic cultured-cells kept on growing, and the number of PD at the last observation under normoxic and hypoxic conditions was 24 and 40, respectively. The theoretically accumulated cell number was 65,000-fold
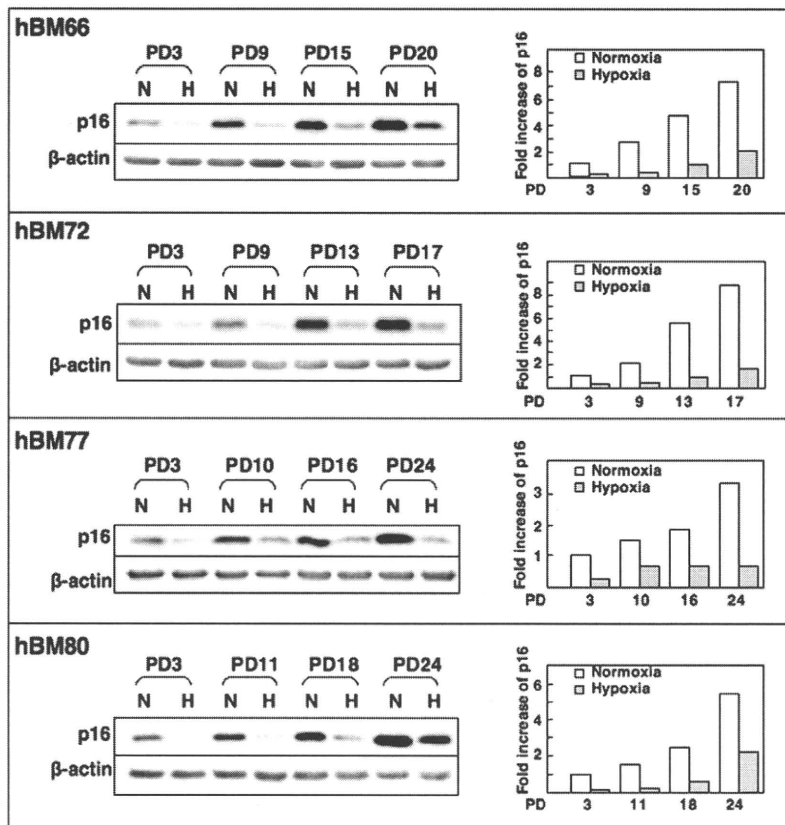

Fig. 2. Hypoxia down-regulated the expression of p16 in MSCs. Expression of p16 was evaluated by Western blotting using antibody for p16 protein. The relative expression level was determined using the value at PD3 of normoxic cultured-cells as a standard. White and gray box indicate normoxic and hypoxic conditions, respectively.

higher in the hypoxic culture. Similar results were obtained with the other three hBM cells (Fig. 1), and the final number of PD in normoxic and hypoxic cultured-cells was 17 and 25 in hBM72, 25 and 39 in hBM77, and 24 and 45 in hBM80.

Hypoxia rescued MSCs from cellular senescence

In the case of hBM77, most of the normoxic cultured-cells at PD25 were positive for SA-β-gal, whereas few were stained in the hypoxic culture at PD28 (Fig. 1B), and the difference was highly significant (Fig. 1C). Similar results were obtained with the other three hBM cells (Fig. 1C), indicating that the hypoxic culture protected MSCs from cellular senescence, which may be the cause of the increase in life span *in vitro*.

Hypoxia inhibited the up-regulation of p16 expression

We have demonstrated that the induction of cellular senescence in MSCs is tightly associated with the up-regulation of *p16* gene expression [20]. Consistent with previous findings, the level of p16 increased with the life span of normoxic cultured-hBM66, which was seven-times higher at PD20 than at PD3 (Fig. 2, upper panel). In contrast, hypoxic cultured-hBM66 retained a lower level

of the p16 expression, which was only two-times higher at PD20 than at PD3 (Fig. 2, upper panel). Similar results were obtained with the other three hBM cells (Fig. 2), suggesting that hypoxia inhibited the induction of *p16* gene expression, which then protected cells from cellular senescence.

Hypoxia affected the ability to differentiate into chondro- and adipogenic, but not osteogenic, lineage

The ability to differentiate into osteo-, chondro-, and adipogenic lineages in the early phase was confirmed in all four hBM cells (data not shown). After long-term culture (about 100 days), no significant difference in osteogenic differentiation, measured based on Ca content, was observed between normoxic and hypoxic cultured-MSCs (Fig. 3A). In contrast, the ability to differentiate into the chondrogenic (Fig. 3B) and adipogenic (Fig. 3C) lineages, measured from GAG and TG content, respectively, was significantly more superior in hypoxic than normoxic conditions.

Hypoxia inhibited the activation of ERK

In the case of hBM66, the expression of molecules related to MAPK signals showed no significant difference between normoxic
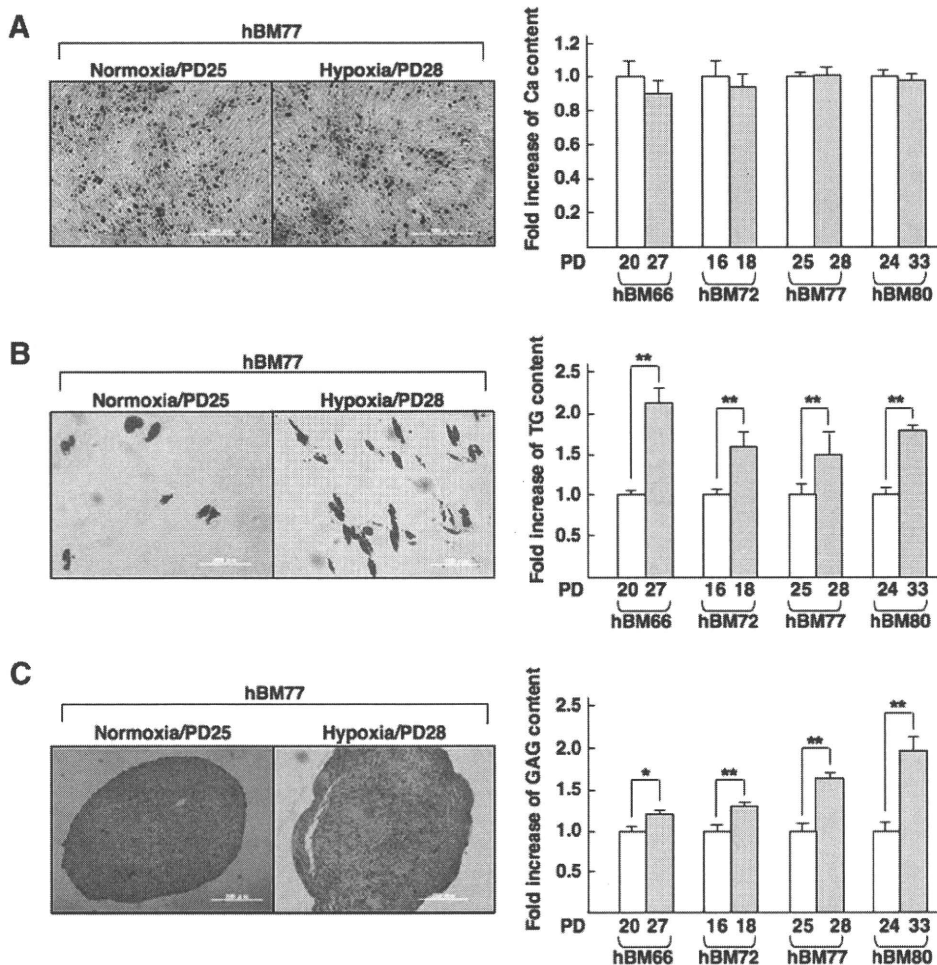

Fig. 3. Hypoxia enhanced differentiation properties of MSCs. Each preparations of MSCs was cultured for approximately 100 days under either normoxic or hypoxic conditions and then induced to undergo (A) osteogenic, (B) chondrogenic, or (C) adipogenic differentiation under normoxic conditions. The results were quantified based on the content of Ca, GAG, or TG, respectively. PD numbers of the MSCs used for these experiments are indicated. White and gray box indicate normoxic and hypoxic conditions, respectively.

and hypoxic cultured-cells except that of ERK (Fig. 4A). Levels of both phospho-ERK1 and phospho-ERK2 were much lower in hypoxic cultured-cells than in normoxic cultured-cells throughout the culture period, and similar results were obtained with the other three hBM cells (Fig. 4B). nPG is an antioxidant, which induces the production HIF-1α protein [24]. Treatment of hBM72 cells (PD3) cultured under normoxic conditions with nPG successfully induced the expression of HIF-1α, but failed to reduce the level of phospho-ERK1/2 (Fig. 4C), indicating that the reduction in phospho-ERK is not a direct consequence of HIF-1α's activation. To investigate the relationship between ERK and p16, the activity of MEK, by which ERK is phosphorylated, was inhibited by U0126. When hBM72 cells (PD3) cultured under normoxic conditions were treated with U0126 for 4 days, activation of ERK was inhibited throughout the culture period (Fig. 4D). During this period, the level of p16 increased two-fold in control cells, but only slightly in U0126 treated-cells (Fig. 4D), suggesting that the ERK signal is one of the factors inducing the expression of the p16 gene.

Discussion

A number of studies have been published regarding the effects of hypoxia on the growth and differentiation of MSCs [12–17], but the results differed considerably. The discrepancies may be at least in part due to differences in species, the concentration of oxygen, and/or the length of culture periods, and the discussion hereafter focuses on the data for human MSCs. As for short-term effects, some studies showed that hypoxia increased the proliferation of MSCs by promoting progression of the cell cycle [16], but others showed no or even the opposite effect [14], consistent with the results of the current study. Two studies have analyzed the long-

term effects of hypoxia on human MSCs. Grayson et al. showed that human MSCs displayed enhanced proliferation under hypoxic conditions (2% pO2) for seven passages over 6 weeks, resulting in a 30-fold increase in cell number compared with that under normoxic conditions [15]. Fehrer et al. showed that MSCs cultured under hypoxic conditions (3% pO2) for up to 100 days had a higher number of final PD than those cultured under normoxic conditions by ten [17], which agreed with the results of the current study. Because the PD time showed no difference during the early phase of growth (Fig. 1A), our data indicate that hypoxia did not affect the growth of cells, but extended their life span, and the marked difference in the number of SA-β-gal-positive cells between hypoxic and normoxic conditions clearly indicates that the lengthening of life span by hypoxia is due to the escape from cellular senescence. We have shown that the up-regulation of p16 gene expression is key to inducing cellular senescence in human MSCs [20]. In the current study, we showed that hypoxia inhibited the up-regulation of p16 gene expression. ROS induces p16 gene expression [21,22], and the p16-Rb pathway then induces the production of ROS, which leads to cellular senescence [25].

Regarding the effects of hypoxia on the differentiation of MSCs, published results vary. To evaluate the ability of MSCs to differentiate, osteo-, chondro-, or adipogenic differentiation has been analyzed in most studies [12–17], but no studies have examined all three lineages in MSCs cultured under hypoxic conditions long term. Martin-Rendon et al. analyzed the short-term effects (24 h) of hypoxia (1% pO2) on the differentiation into three lineages and found that only chondrogenic differentiation was improved [16]. Our data indicated that chondrogenic, as well as adipogenic, but not osteogenic, differentiation was improved in MSCs cultured under hypoxic conditions for long term (about 100 days). Although
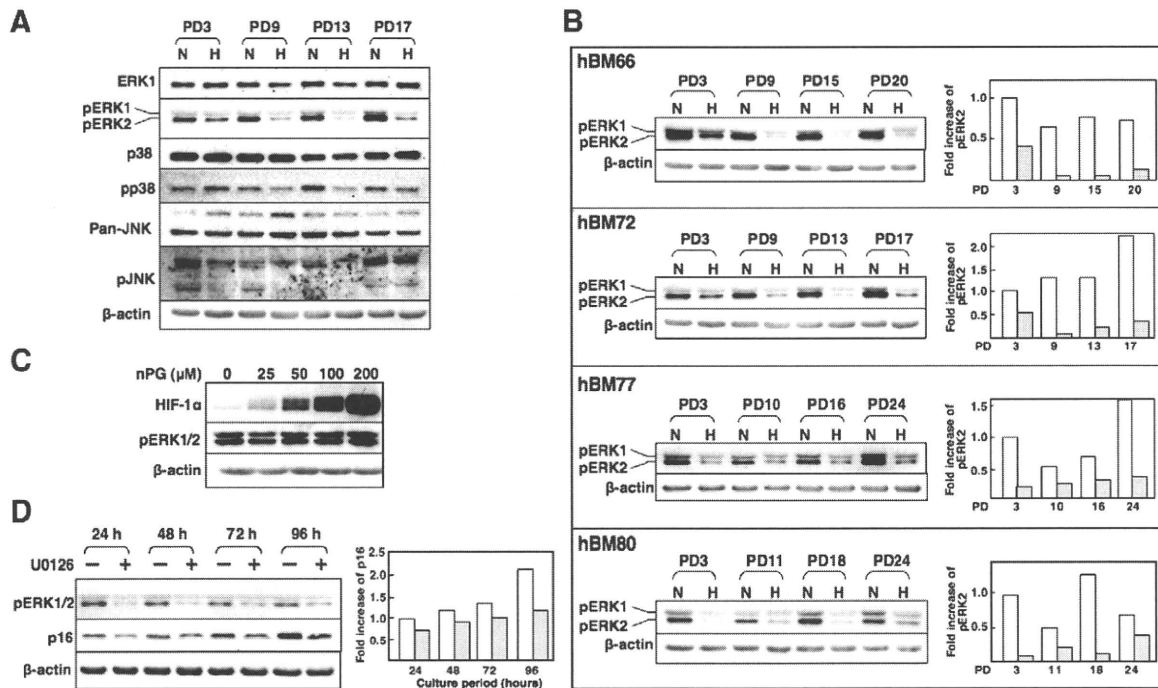

Fig. 4. Hypoxia down-regulated the activation of ERK in MSCs. (A) Expression of molecules related to MAPK signaling pathways of huBM72 at the indicated PD. (B) Expression of pERK1/2 during the life span of MSCs in vitro. The relative level of pERK2 was determined using the value at PD3 of normoxic cells as a standard. White and gray box indicate normoxic and hypoxic conditions, respectively. (C) Effect of nPG treatment on the expression of HIF-1α and pERK1/2. huBM72 cells cultured under normoxic conditions at PD3 were treated with nPG at the indicated concentration for 4 h, and proteins were extracted for Western blotting. (D) Effect of a MEK inhibitor on the expression of pERK1/2 and p16. huBM72 cells cultured under normoxic conditions at PD3 were treated with U0126 (10 μM) for up to 96 h, and proteins were extracted for Western blotting. The relative expression level of p16 was determined using the value of normoxic cultured-cells at 24 h as a standard. White and gray box indicate normoxic and hypoxic conditions, respectively.

the molecular mechanisms underlying this change in the behavior of MSCs are not known, the down-regulation of phospho-ERK expression caused by a reduction in oxygen is an intriguing new finding of the current study. MAPK signaling pathways have profound effects on the growth and differentiation of MSCs [26,27], and the signaling through ERK has been investigated intensively. Activation of the ERK signal triggers osteogenic differentiation [28,29]. The up-regulation of MAPK signals promoted chondrogenesis by inducing the expression of the *Sox9* gene [30]. The inhibition of ERK signals reduced the adipogenic differentiation [31]. Therefore, the ERK signal is essential to the differentiation of MSCs. In other words, inhibition of the ERK signal may restrict the "spontaneous" differentiation which maintains MSC in an undifferentiated state. The ERK signal also plays a role as a mitogenic stimulus, which promotes growth, but at the same time induces cellular senescence of MSCs. Inhibition of the ERK signal by a MEK inhibitor reduced the up-regulation of *p16* gene expression. Therefore, down-regulation of phospho-ERK expression may also help cells to escape from cellular senescence during propagation *in vitro*. Further study of mechanisms by which hypoxia down-regulates the ERK signal may provide a new method of culturing MSCs.

Acknowledgments

References

[1] A.I. Caplan, S.P. Bruder, Mesenchymal stem cells: building blocks for molecular medicine in the 21st century, Trends Mol. Med. 7 (2001) 259–264.

[2] L. Mazzini, K. Mareschi, I. Ferrero, E. Vassallo, G. Oliveri, R. Boccaletti, L. Testa, S. Livigni, F. Fagioli, Autologous mesenchymal stem cells: clinical applications in amyotrophic lateral sclerosis, Neurol. Res. 28 (2006) 523–526.

[3] H. Ohgushi, N. Kotobuki, H. Funaoka, H. Machida, M. Hirose, Y. Tanaka, Y. Takakura, Tissue engineered ceramic artificial joint-ex vivo osteogenic differentiation of patient mesenchymal cells on total ankle joints for treatment of osteoarthritis, Biomaterials 26 (2005) 4654–4661.

[4] W. Wagner, P. Horn, M. Castoldi, A. Diehlmann, S. Bork, R. Saffrich, V. Benes, J. Blake, S. Pfister, V. Eckstein, A.D. Ho, Replicative senescence of mesenchymal stem cells: a continuous and organized process, PLoS ONE 3 (2008) e2213.

[5] K. Itahana, J. Campisi, G.P. Dimri, Mechanisms of cellular senescence in human and mouse cells, Biogerontology 5 (2004) 1–10.

[6] S. Loft, P. Hogh Danielsen, L. Mikkelsen, L. Risom, L. Forchhammer, P. Moller, Biomarkers of oxidative damage to DNA and repair, Biochem. Soc. Trans. 36 (2008) 1071–1076.

[7] P.A. Zuk, M. Zhu, H. Mizuno, J. Huang, J.W. Futrell, A.J. Katz, P. Benhaim, H.P. Lorenz, M.H. Hedrick, Multilineage cells from human adipose tissue: implications for cell-based therapies, Tissue Eng. 7 (2001) 211–228.

[8] C. De Bari, F. Dell'Accio, P. Tylzanowski, F.P. Luyten, Multipotent mesenchymal stem cells from adult human synovial membrane, Arthritis Rheum. 44 (2001) 1928–1942.

[9] G. Kogler, S. Sensken, J.A. Airey, T. Trapp, M. Muschen, N. Feldhahn, S. Liedtke, R.V. Sorg, J. Fischer, C. Rosenbaum, S. Greschat, A. Knipper, J. Bender, O. Degistirici, J. Gao, A.I. Caplan, E.J. Colletti, G. Almeida-Porada, H.W. Muller, E. Zanjani, P. Wernet, A new human somatic stem cell from placental cord blood with intrinsic pluripotent differentiation potential, J. Exp. Med. 200 (2004) 123–135.

[10] S. Bajada, I. Mazakova, J.B. Richardson, N. Ashammakhi, Updates on stem cells and their applications in regenerative medicine, J. Tissue Eng. Regen. Med. 2 (2008) 169–183.

[11] D.C. Chow, L.A. Wenning, W.M. Miller, E.T. Papoutsakis, Modeling pO(2) distributions in the bone marrow hematopoietic compartment. II. Modified Kroghian models, Biophys. J. 81 (2001) 685–696.

[12] D.P. Lennon, J.M. Edmison, A.I. Caplan, Cultivation of rat marrow-derived mesenchymal stem cells in reduced oxygen tension: effects on in vitro and in vivo osteochondrogenesis, J. Cell. Physiol. 187 (2001) 345–355.

[13] H. Ren, Y. Cao, Q. Zhao, J. Li, C. Zhou, L. Liao, M. Jia, H. Cai, Z.C. Han, R. Yang, G. Chen, R.C. Zhao, Proliferation and differentiation of bone marrow stromal cells under hypoxic conditions, Biochem. Biophys. Res. Commun. 347 (2006) 12–21.

[14] W.L. Grayson, F. Zhao, R. Izadpanah, B. Bunnell, T. Ma, Effects of hypoxia on human mesenchymal stem cell expansion and plasticity in 3D constructs, J. Cell. Physiol. 207 (2006) 331–339.

[15] W.L. Grayson, F. Zhao, B. Bunnell, T. Ma, Hypoxia enhances proliferation and tissue formation of human mesenchymal stem cells, Biochem. Biophys. Res. Commun. 358 (2007) 948–953.

[16] E. Martin-Rendon, S.J. Hale, D. Ryan, D. Baban, S.P. Forde, M. Roubelakis, D. Sweeney, M. Moukayed, A.L. Harris, K. Davies, S.M. Watt, Transcriptional profiling of human cord blood CD133+ and cultured bone marrow mesenchymal stem cells in response to hypoxia, Stem Cells 25 (2007) 1003–1012.

[17] C. Fehrer, R. Brunauer, G. Laschober, H. Unterluggauer, S. Reitinger, F. Kloss, C. Gully, R. Gassner, G. Lepperdinger, Reduced oxygen tension attenuates differentiation capacity of human mesenchymal stem cells and prolongs their lifespan, Aging Cell 6 (2007) 745–757.

[18] A.V. Molofsky, S.G. Slutsky, N.M. Joseph, S. He, R. Pardal, J. Krishnamurthy, N.E. Sharpless, S.J. Morrison, Increasing p16INK4a expression decreases forebrain progenitors and neurogenesis during ageing, Nature 443 (2006) 448–452.

[19] V. Janzen, R. Forkert, H.E. Fleming, Y. Saito, M.T. Waring, D.M. Dombkowski, T. Cheng, R.A. DePinho, N.E. Sharpless, D.T. Scadden, Stem-cell ageing modified by the cyclin-dependent kinase inhibitor p16INK4a, Nature 443 (2006) 421–426.

[20] K.R. Shibata, T. Aoyama, Y. Shima, K. Fukiage, S. Otsuka, M. Furu, Y. Kohno, K. Ito, S. Fujibayashi, M. Neo, T. Nakayama, T. Nakamura, J. Toguchida, Expression of the p16INK4A gene is associated closely with senescence of human mesenchymal stem cells and is potentially silenced by DNA methylation during in vitro expansion, Stem Cells 25 (2007) 2371–2382.

[21] D.G. Yang, L. Liu, X.Y. Zheng, Cyclin-dependent kinase inhibitor p16INK4a and telomerase may co-modulate endothelial progenitor cells senescence, Ageing Res. Rev. 7 (2008) 137–146.

[22] T. Okamoto, T. Aoyama, T. Nakayama, T. Nakamata, T. Hosaka, K. Nishijo, T. Nakamura, T. Kiyono, J. Toguchida, Clonal heterogeneity in differentiation potential of immortalized human mesenchymal stem cells, Biochem. Biophys. Res. Commun. 295 (2002) 354–361.

[23] M.F. Pittenger, A.M. Mackay, S.C. Beck, R.K. Jaiswal, R. Douglas, J.D. Mosca, M.A. Moorman, D.W. Simonetti, S. Craig, D.R. Marshak, Multilineage potential of adult human mesenchymal stem cells, Science 284 (1999) 143–147.

[24] F. Tsukiyama, Y. Nakai, M. Yoshida, T. Tokuhara, K. Hirota, A. Sakai, H. Hayashi, T. Katsumata, Gallate, the component of HIF-inducing catechins, inhibits HIF prolyl hydroxylase, Biochem. Biophys. Res. Commun. 351 (2006) 234–239.

[25] A. Takahashi, N. Ohtani, K. Yamakoshi, S. Iida, H. Tahara, K. Nakayama, K.I. Nakayama, T. Ide, H. Saya, E. Hara, Mitogenic signalling and the p16INK4a-Rb pathway cooperate to enforce irreversible cellular senescence, Nat. Cell Biol. 8 (2006) 1291–1297.

[26] I. Carcamo-Orive, N. Tejados, J. Delgado, A. Gaztelumendi, D. Otaegui, V. Lang, C. Trigueros, ERK2 protein regulates the proliferation of human mesenchymal stem cells without affecting their mobilization and differentiation potential, Exp. Cell Res. 314 (2008) 1777–1788.

[27] R.K. Jaiswal, N. Jaiswal, S.P. Bruder, G. Mbalaviele, D.R. Marshak, M.F. Pittenger, Adult human mesenchymal stem cell differentiation to the osteogenic or adipogenic lineage is regulated by mitogen-activated protein kinase, J. Biol. Chem. 275 (2000) 9645–9652.

[28] S. Peng, G. Zhou, K.D. Luk, K.M. Cheung, Z. Li, W.M. Lam, Z. Zhou, W.W. Lu, Strontium promotes osteogenic differentiation of mesenchymal stem cells through the Ras/MAPK signaling pathway, Cell. Physiol. Biochem. 23 (2009) 165–174.

[29] J. Liu, Z. Zhao, J. Li, L. Zou, C. Shuler, Y. Zou, X. Huang, M. Li, J. Wang, Hydrostatic pressures promote initial osteodifferentiation with ERK1/2 not p38 MAPK signaling involved, J. Cell. Biochem. 107 (2009) 224–232.

[30] Y. Chang, S.W. Ueng, S. Lin-Chao, C.C. Chao, Involvement of Gas7 along the ERK1/2 MAP kinase and SOX9 pathway in chondrogenesis of human marrow-derived mesenchymal stem cells, Osteoarthritis Cartilage 16 (2008) 1403–1412.

[31] Q.C. Liao, Y.L. Li, Y.F. Qin, L.D. Quarles, K.K. Xu, R. Li, H.H. Zhou, Z.S. Xiao, Inhibition of adipocyte differentiation by phytoestrogen genistein through a potential downregulation of extracellular signal-regulated kinases 1/2 activity, J. Cell. Biochem. 104 (2008) 1853–1864.

Histone Modifiers, YY1 and p300, Regulate the Expression of Cartilage-specific Gene, Chondromodulin-I, in Mesenchymal Stem Cells*[s]

Tomoki Aoyama[‡§¶], Takeshi Okamoto[‡§], Kenichi Fukiage[‡§], Seiji Otsuka[‡||], Moritoshi Furu[‡§], Kinya Ito[‡||], Yonghui Jin[‡], Michiko Ueda[‡], Satoshi Nagayama**, Tomitaka Nakayama[§], Takashi Nakamura[§], and Junya Toguchida[‡§‡‡1]

From the [‡]Institute for Frontier Medical Sciences, the [‡‡]Center for iPS Cell Research and Application, Kyoto University, Kyoto 606-8507, the [§]Department of Orthopaedic Surgery, [¶]Human Health Sciences, and the **Department of Surgery and Surgical Basic Science, Graduate School of Medicine, Kyoto University, Kyoto 606-8507, Japan and the [||]Department of Musculoskeletal Medicine, Graduate School of Medical Sciences, Nagoya City University, Nagoya 467-8601, Japan

Elucidating the regulatory mechanism for tissue-specific gene expression is key to understanding the differentiation process. The chondromodulin-I gene (ChM-I) is a cartilage-specific gene, the expression of which is regulated by the transcription factor, Sp3. The binding of Sp3 to the core-promoter region is regulated by the methylation status of the Sp3-binding motif as we reported previously. In this study, we have investigated the molecular mechanisms of the down-regulation of ChM-I expression in mesenchymal stem cells (MSCs) and normal mesenchymal tissues other than cartilage. The core-promoter region of cells in bone and peripheral nerve tissues was hypermethylated, whereas the methylation status in cells of other tissues including MSCs did not differ from that in cells of cartilage, suggesting the presence of inhibitory mechanisms other than DNA methylation. We found that a transcriptional repressor, YY1, negatively regulated the expression of ChM-I by recruiting histone deacetylase and thus inducing the deacetylation of associated histones. As for a positive regulator, we found that a transcriptional co-activator, p300, bound to the core-promoter region with Sp3, inducing the acetylation of histone. Inhibition of YY1 in combination with forced expression of p300 and Sp3 restored the expression of ChM-I in cells with a hypomethylated promoter region, but not in cells with hypermethylation. These results suggested that the expression of tissue-specific genes is regulated in two steps; reversible down-regulation by transcriptional repressor complex and tight down-regulation via DNA methylation.

The expression of cell lineage-specific genes is a key to initiating the differentiation of stem cells into a particular cell lineage, and the down-regulation of such genes in cells of other

lineages is also critical to maintain a normal cellular physiology. The chondromodulin-I (ChM-I)[2] gene is a specific gene for cartilage tissue (1). We have found that the basal promoter activity of ChM-I is driven by a ubiquitous transcription factor, Sp3, and chondrocyte-specific expression is regulated by the methylation status of the Sp3-binding motif in the core-promoter region (2). Demethylation treatment in vitro restored the expression of ChM-I in cells of the osteogenic lineage (2, 3). A similar result was obtained with cells of the adipogenic lineage, in which the expression of an adipocyte-specific gene was restored in non-adipogenic cells by the elimination of methylated DNA in a regulatory region (4). Because DNA methylation is considered a tight epigenetic change under physiological conditions, it is a suitable mechanism for cells to inhibit the expression of unnecessary genes. It is, however, still to be investigated whether cells in tissues other than cartilage share the same inhibitory mechanism. It is also important to know how the expression of lineage-specific genes is down-regulated in tissue stem cells before differentiation is initiated. Mesenchymal stem cells (MSCs) in bone marrow are tissue stem cells, which can differentiate into multiple mesenchymal cell lineages including chondrogenic cells (5, 6). Because three-dimensional cultures supplemented with growth factors such as TGF-β can induce the chondrogenic differentiation of MSCs (6), there should be a mechanism other than DNA methylation to down-regulate the gene expression of ChM-I in undifferentiated MSCs. Modification of the histone tail is another mechanism regulating gene expression. The acetylation of histone H3 and H4 promotes gene expression, whereas deacetylation inhibits the expression (7). The dimethylation of histone H3 at lysine 9 (H3K9) in particular is correlated with DNA methylation and markedly inhibits gene expression (8, 9). These modifications of the histone tail and methylation status determine differentiation (10), and are regulated by several intrinsic histone modifiers including p300 and YY1 (11–13). p300 possesses intrinsic histone acetyltransferase (HAT) activity (11, 12). YY1 is a member of the polycomb group of transcription factors, which establish and maintain transcrip-

[s] The on-line version of this article (available at http://www.jbc.org) contains supplemental Figs. S1 and S2.

[1] To whom correspondence should be addressed: Institute for Frontier Medical Sciences, Kyoto University, 53 Kawahara-cho, Shogoin, Sakyo-ku, Kyoto 606-8507, Japan. Tel.: 81-75-751-4134; Fax: 81-75-751-4646; E-mail: togjun@frontier.kyoto-u.ac.jp.

[2] The abbreviations used are: ChM, chondromodulin; MSC, mesenchymal stem cell; HAT, histone acetyltransferase; HDAC, histone deacetylase; OND, oligonucleotides.

tional silencing by recruiting histone deacetylase (HDAC) (13, 14). These intrinsic factors regulate the epigenetic status and regulate gene expression.

Here we demonstrated that the down-regulation of *ChM-I* expression by DNA methylation is restricted in particular cell types, whereas other cells including MSCs are free from the methylation, and found that expression of the *ChM-I* gene in these cells is reversibly dependent on histone modifications, which are regulated by the net activity of intrinsic histone modifiers, YY1 and p300.

EXPERIMENTAL PROCEDURES

Tissue Specimens and Primary Cultured Cells—Mesenchymal (cartilage, bone, fat, muscle, ligament, and tendon) and non-mesenchymal tissues (nerve, artery, and skin) were obtained from the lower limb of a 56-year-old male who underwent above-knee amputation. The tissues were frozen by dry ice and kept at $-80\,°C$ until nucleic acid extraction. Human primary cultured chondrocytes (hPCs) was isolated from same patient and cultured as previously mentioned (15). MSCs were isolated from the iliac bone of healthy donor as described (16). Normal human osteoblasts (NHOSTs) and human primary pre-adipocytes (hPAs) were obtained from TaKaRa (TaKaRa Bio, Shiga, Japan). All the primary cells were maintained in DMEM (Sigma-Aldrich) with 10% fetal bovine serum (Thermo Fisher Scientific Inc., Waltham, MA), 100 units/ml penicillin, and 100 mg/ml streptomycin, in 5% CO_2 at 37 °C. The Ethics Committee of the Faculty of Medicine, Kyoto University, approved the procedure and informed consent was obtained.

Cell Lines and Culture Conditions—The human cell lines, Saos2, were obtained from American Type Culture Collection (ATCC; Manassas, VA). The human osteosarcoma cell lines TAKAO and ANOS were established in our laboratory (2). All the cell lines used in this study were maintained in DMEM (Sigma-Aldrich) with 10% fetal bovine serum (Thermo Fisher Scientific Inc.), 100 units/ml penicillin, and 100 mg/ml streptomycin, in 5% CO_2 at 37 °C.

Antibodies and Expression Vectors—The following antibodies were used; anti-YY1 (sc-7341, Santa Cruz Biotechnology, Santa Cruz, CA), anti-p300 (05–257, Millipore Corp, Billerica, MA), anti-Sp3 (sc-644, Santa Cruz Biotechnology), anti-acetylated H3K9 (06–942, Millipore Corp), anti-dimethylated H3K9 (07–212, Millipore Corp), anti-pan H3 (07–690, Millipore Corp), and anti-HDAC2 (51–5100, Zymed Laboratory Inc., San Francisco, CA). Expression vectors for YY1 (pCEP-YY1) and p300 (pcDNA3-p300) were kindly provided by Drs. E. Seto and K. Miyazono, respectively. The Sp3 expression vector (pCMV-Sp3) was previously described elsewhere (17).

Reverse Transcription (RT)-PCR and Quantitative RT-PCR—RNA was isolated using the Rneasy kit (Qiagen KK, Tokyo, Japan) from frozen tissues and the cultured cell lines. All RT reactions were performed using 1 μg of total RNA with a Super Script First Strand Synthesis System for RT-PCR kit (Invitrogen, Carlsbad, CA). The relative amount of *ChM-I* mRNA was assessed by TaqMan real-time PCR with the ABI PRISM 7700 sequence detection system (Applied Biosystems, Foster City, CA) (2). A75-bp fragment from +411 (exon 4) to +485 (exon 5) of the *ChM-I* cDNA (GenBank™ accession number XM_007132) was amplified using specific primers (sense, 5′-GAAGGCTCGTATTCCTGAGGTG-3′; antisense, 5′-TGGCATGATCTTGCCTTCCAGT-3′) and labeled with a TaqMan probe (5′-FAM-CGTGACCAAACAGAGCATCTC-CTCCA-3′-TAMRA). 18 S rRNA was used as the internal control, and all reactions were run in duplicate. The ratio of *ChM-I*/18 S in each sample was calculated, and the expression level of *ChM-I* genes was demonstrated as a relative value using the *ChM-I*/18 S ratio in human articular cartilage as a standard (1.0) (2).

Drug Treatment—Cells (1×10^5) were seeded on 60-mm dishes in DMEM with 10% FBS. After they had attached to the dish, the cells were treated with either 5-*aza*-2′-deoxycytidine (5-*aza*-dC; Sigma-Aldrich) (1 μM) for 96 h or MS-275 (Nihon Scherring K.K., Chiba, Japan) (1 μM) for 24 h.

Bisulfite Genomic Sequencing—The bisulfite modification of DNA samples was performed using the EpiTect bisulfite kit (Qiagen). DNA (1 μg) was digested by BamHI for 12 h and subjected to sodium bisulfite treatment. Bisulfite-modified DNA-spanning residues -297 to -104 relative to the transcription start point (2) was amplified, cloned into the TA-vector (Invitrogen), and sequenced using an ABI 377 semiautomatic sequencer (Applied Biosystems).

Electrophoresis Mobility Shift Assay (EMSA)—Double-stranded DNA fragments corresponding to the sequence from -357 to -333 and from -86 to -44 were synthesized by annealing two single-stranded oligonucleotides (OND) (5′-CTTCACCTTCCATGAGCCATCTTC-3′ and 5′-GGGGGA-AGATGGCTCATGGAAGGT-3′; 5′-GGGCATCCGGGAG-TGCAGGACGAGCTTCCCGCGGCGGGA-3′; and 5′-TCT-CTCCCGCCGCGGGAAGCTCGTCCTGCACTCCCGGAT-3′, respectively) and filling in by DNA polymerase I (TOYOBO, Osaka, Japan). These fragments were designated GR3 and GR4 (Fig. 2*B*). For the formation of the complex, 5 μg of nuclear extract from cell lysate was incubated with ^{32}P end-labeled ONDs for 20 min at room temperature. The mixtures were electrophoresed in 5% polyacrylamide gel in 0.5× Tris borate EDTA at 45 volts for 3 h, and the gel then was dried and autoradiographed. For the competition assay, the OND-protein complex was produced in the same way in the presence of given amounts of non-labeled OND. In the supershift assay, nuclear extracts were incubated with 1 μg of anti-YY1 and anti-p300 antibody for 1 h on ice before being mixed with labeled DNA.

Luciferase Assay—The 533-bp fragment from -446 to $+86$ and 383-bp fragment from -296 to $+86$ relative to the transcription initiation site of the *ChM-I* gene was amplified by PCR, and cloned into a TA-vector using the TOPO cloning kit (Invitrogen). These fragments were subcloned into the luciferase reporter plasmid, PGV-B (Toyo Ink, Tokyo, Japan), yielding PGV-B-f1 and PGV-B-f1-del. Two tandem binding motifs of YY1 (*CCAT*) was mutated to (*TTAT*) by PCR, cloned into PGV-B, and designated PGV-B-f1-mt. One microgram of each reporter plasmid was co-transfected with 1 μg of pCEP-YY1 or pCMV-p300. Transfection efficiency was standardized by the co-transfection of 1 ng of pRL-TK control vector (Toyo Ink). Cells were harvested 24 h after transfection, and luciferase assays were performed with the

— 132 —

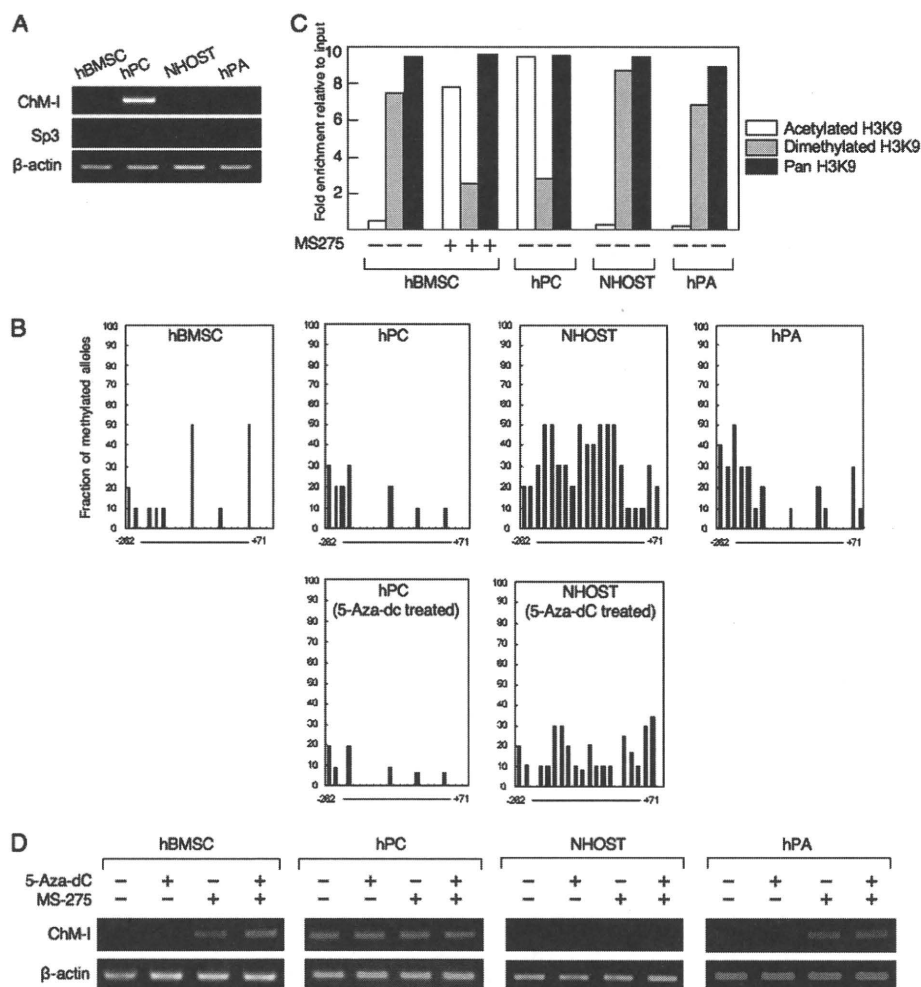## Histone Modifiers Regulate Cartilage-specific Gene

FIGURE 1. **DNA methylation and histone deacetylation down-regulate the expression of *ChM-I* in a cell type-specific manner.** *A*, expression of the *ChM-I* and *Sp3* genes in primary cultured mesenchymal cells. *B*, methylation status of the core-promoter region of *ChM-I*. The methylation of each CpG site was analyzed in 10 alleles by bisulfite genomic sequencing. The *y*-axis indicates the fraction of methylated alleles and the *x*-axis indicates the position of each CpG site relative to the transcription start site. Methylation status in hPC and NHOST treated with a demethylating reagent (5-*aza*-dC, 1 μM for 96 h) were also shown. *C*, ChIP-qPCR assay for the modification of histones in primary cultured mesenchymal cells. *Open box*, acetylated H3K9; *closed box*, dimethylated H3K9; *gray box*, Pan H3. Histone modification in hBMSC treated with an HDAC inhibitor (MS-275, 1 μM for 24 h) were also shown. The *y*-axis represents fold enrichment relative to input. *D*, expression of *ChM-I* after treatment with 5-*aza*-dC and/or MS-275.

tenth of the sample was set aside as an input control, and the rest was precleared with salmon sperm DNA protein A-Sepharose beads (Millipore Corp) for 30 min with agitation. The soluble chromatin fraction was collected with each antibody at 4 °C overnight with rotation. Immune complexes were collected with salmon sperm DNA protein A-Sepharose beads and washed with the manufacturer's low salt, high salt, and LiCl buffers and then washed twice with TE buffer (10 mM Tris-HCl and 1 mM EDTA). The chromatin-antibody complexes were eluted with elution buffer (1% SDS and 0.1 M NaHCO$_3$). Protein DNA cross-links were reversed with 5 M NaCl at 65 °C for 4 h, proteinase K treatment and phenol-chloroform extraction were carried out, and then the DNA was precipitated in ethanol. The DNA pool from ChIP, input control and negative control was used for quantitative PCR. PCR amplification was performed on an ABI 7700 real-time PCR (Applied Biosystems). PCR amplification was performed using primers specific for the *ChM-I* regulatory region (sense, 5'-GAA-TGCAGGCCAGTGAGAAGGT-3';1 antisense, 5'-GCACCCTGGG-ATCTGTCCCGCT-3', Fig. 2*B*). The PCR conditions were an initial step of 5 min at 95 °C, followed by 40 cycles of 15 s at 95 °C, 10 s at 64 °C and 60 s at 72 °C. Primers were designed according to the selected genes for evaluating ChIP. To generate a standard curve for each

PicaGene Dual SeaPansy system (Toyo Ink). Firefly-luciferase activity and SeaPansy-luciferase activity were measured as relative light units with a luminometer (STRATEC Biomedical Systems, Birkenfeld, Deutschland). The fold increase was calculated based on empty vector activity. Each experiment was performed in triplicate.

Chromatin Immunoprecipitation-Quantitative Polymerase Chain Reaction—The suitability of each antibody for the ChIP assay was confirmed by immunoprecipitation-Western blotting (data not shown). Tissue samples were treated using an EpiQuik tissue ChIP kit (Epigentek Group Inc. Brooklyn, NY). Cells were harvested and mixed with formaldehyde at a final concentration of 1.0% for 10 min at 37 °C to cross-link protein to DNA. Cells then were suspended in 0.2 ml of SDS lysis buffer and settled on ice for 10 min. DNA cross-linked with protein was sonicated into fragments of 200–1,000 bp. One-

amplicon, threshold cycle (CT) values of serially diluted input DNA, which were extracted in the ChIP experiment, were determined. The status of histone modification and binding of HDAC2, p300, YY1, and Sp3 changes were determined using the 2(-Delta Delta C(T)) method (18). They were demonstrated as a relative value using the enrichment of IP DNA/input DNA. A melting curve analysis was performed for each reaction to ensure a single peak. Each experiment was performed in triplicate, with the values averaged to obtain 1 datum per sample.

siRNAs—Luciferase siRNA duplex (GL2RN1, Dharmacon) was used as a negative control. 40 μM siRNA for YY1 (GeneSolution siRNA; Hs-YY1–5, Qiagen), p300 (p300 Pub. siRNA, Duplex1, Qiagen), and Sp3 (previously described in (2)) were transfected by Lipofection LTX (Invitrogen). RNA was prepared 48 h after transfection and used for the RT-PCR.
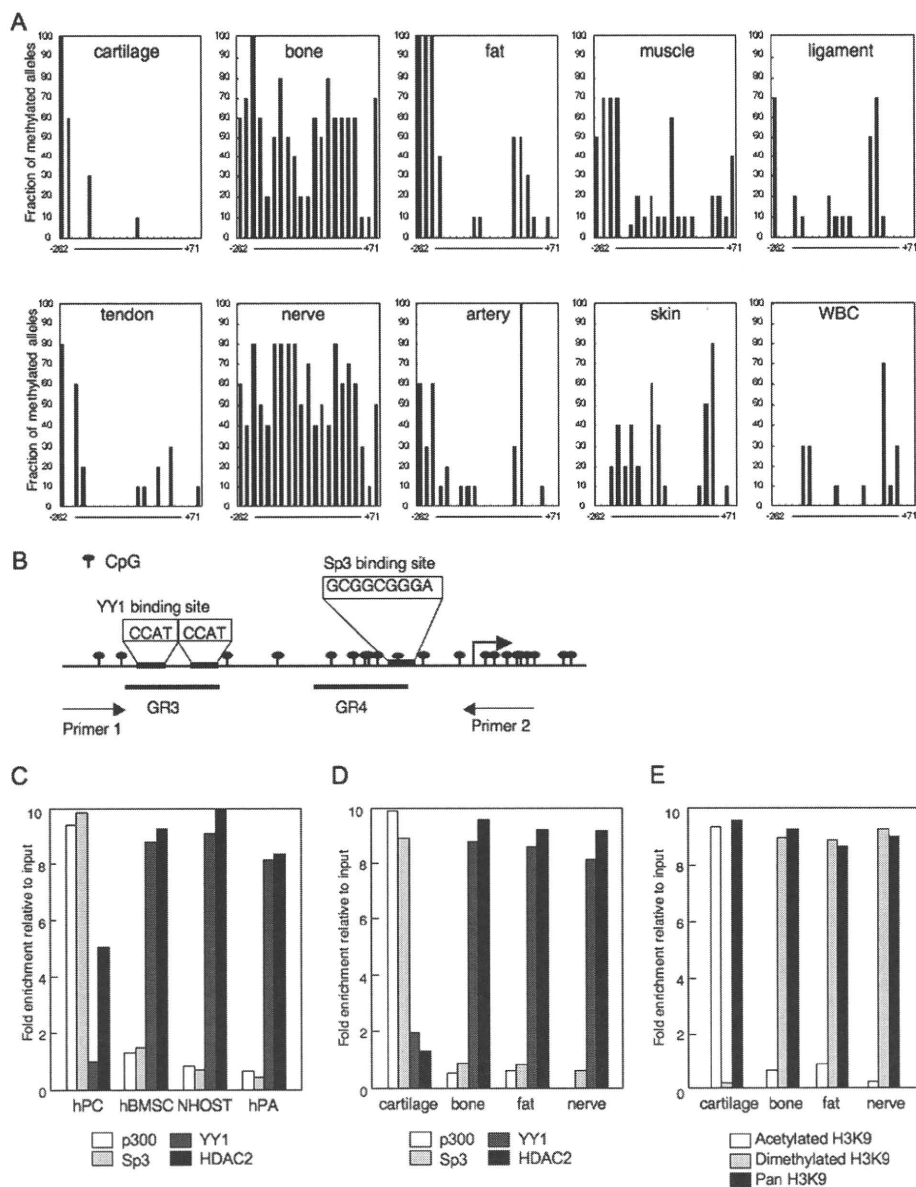
− 133 −

FIGURE 2. **Binding of YY1 and p300 determined the modification of H3K9 and the mRNA expression of ChM-I in mesenchymal tissues.** A, methylation status of the core-promoter region of the *ChM-I*. DNA extracted from normal tissue was analyzed by bisufite genomic sequencing. B, genomic structure of the core-promoter region of *ChM-I*. CpG sites from −262 to +71 were marked as indicated, and the transcription start site is indicated by an *arrow*. Two overlapping YY1-binding motifs (−344 to −347 and −342 to −346), and an Sp3-binding motifs (−56 to −48) are also indicated. A DNA fragment for the ChIP assay was amplified by primer 1 (−446 to −425) and primer 2 (+70 to +91). GR3 (−357 to −337) and GR4 (−86 to −44) were OND probes used in the EMSA for YY1 and p300, respectively. ChIP-qPCR assay for the binding of transcriptional regulators in primary cultured cells (C) and cells of normal tissues (D). The *y*-axis represents fold enrichment relative to input. E, ChIP-qPCR assay for the modification of histones in normal tissues.

sion levels of the *Sp3* gene did not differ among the four types of cells (Fig. 1A). The core-promoter region of *ChM-I* was hypomethylated in hPCs and hypermethylated in NHOSTs (Fig. 1B), which was consistent with the positive and negative expression of *ChM-I* in each cell. The methylation status of the core-promoter region of hMSCs or hPAs, however, was not significantly different from that of hPCs in spite that the expression of *ChM-I* was not detected in these cells (Fig. 1B). We have also shown that the acetylation of histone H3 at lysine 9 (H3K9) is necessary to induce the binding of Sp3 to the core-promoter region of *ChM-I*. ChIP analyses showed that H3K9 associated with the core-promoter region was acetylated in hPCs, but dimethylated in hMSCs, NHOSTs, and hPAs (Fig. 1C). Treatment with a demethylation reagent (5-*aza*-dC) induced the expression of *ChM-I* in NHOSTs (Fig. 1D), which was associated with demethylatiion in the promoter region of the *ChM-I* gene (Fig. 1B, *lower panel*). 5-*aza*-dC treatment, however, showed no effects in hMSCs or hPAs (Fig. 1D). On the other hand, treatment with a HDAC inhibitor (MS-275) induced the expression of *ChM-I* gene in hMSCs and hPAs, but not in NHOSTs (Fig. 1D). The induction of ChM-1 gene expression in hMSC was associated with the acetylation of H3K9 (Fig. 1C). These results suggested two mechanisms for the down-regulation of *ChM-I* expression in primary-cultured cells; methylation of the core-promoter region as found in NHOSTs, and histone deacetylation and methylation without DNA methylation as found in hMSCs and hPAs.

The Binding of YY1 and p300 Correlates to the Expression of ChM-I in Normal Mesenchymal Tissues—Among the normal mesenchymal tissues examined, the expression of *ChM-I* was observed only in cartilage (supplemental Fig. S1). The methylation status of the core-promoter region, however, differed significantly among tissues (Fig. 2A). DNA extracted from cells in cartilage and fat tissues showed a hypomethylated state in the core-promoter region, which was similar to those found in hPCs and hPAs (Fig. 1B). DNA extracted from cells in bone and nerve tissues showed

RESULTS

DNA Methylation and Histone Deacetylation Down-regulate the Expression of ChM-I in a Cell Type-specific Manner—The expression of *ChM-I* was analyzed by RT-PCR in primary-cultured mesenchymal cells (hMSCs, hPCs, NHOSTs, and hPAs), among which only hPCs expressed the gene (Fig. 1A). We have previously shown the expression of *ChM-I* to be induced by the binding of Sp3, which was regulated by the methylation status of the binding motif in the core-promoter region (2). Expres-